Bio-Design and Manufacturing (2021) 4:311–343
https://doi.org/10.1007/s42242-020-00112-5

REVIEW

3D printed microfluidic devices: a review focused on four fundamental manufacturing approaches and implications on the field of healthcare

Viraj Mehta[1] · Subha N. Rath[1]

Received: 28 August 2020 / Accepted: 11 November 2020 / Published online: 3 January 2021

Abstract

In the last few years, 3D printing has emerged as a promising alternative for the fabrication of microfluidic devices, overcoming some of the limitations associated with conventional soft-lithography. Stereolithography (SLA), extrusion-based technology, and inkjet 3D printing are three of the widely used 3D printing technologies owing to their accessibility and affordability. Microfluidic devices can be 3D printed by employing a manufacturing approach from four fundamental manufacturing approaches classified as (1) direct printing approach, (2) mold-based approach, (3) modular approach, and (4) hybrid approach. To evaluate the feasibility of 3D printing technologies for fabricating microfluidic devices, a review focused on 3D printing fundamental manufacturing approaches has been presented. Using a broad spectrum of additive manufacturing materials, 3D printed microfluidic devices have been implemented in various fields, including biological, chemical, and material synthesis. However, some crucial challenges are associated with the same, including low resolution, low optical transparency, cytotoxicity, high surface roughness, autofluorescence, non-compatibility with conventional sterilization methods, and low gas permeability. The recent research progress in materials related to additive manufacturing has aided in overcoming some of these challenges. Lastly, we outline possible implications of 3D printed microfluidics on the various fields of healthcare such as in vitro disease modeling and organ modeling, novel drug development, personalized treatment for cancer, and cancer drug screening by discussing the current state and future outlook of 3D printed 'organs-on-chips,' and 3D printed 'tumor-on-chips.' We conclude the review by highlighting future research directions in this field.

Keywords 3D printing · Additive manufacturing · Microfluidics · Lab-on-a-chip · Organ-on-a-chip · Tumor-on-a-chip

Introduction

Microfluidic devices have played a key role in deciphering numerous biological phenomena [1, 2]. Various microfluidic designs are available, which can be used for recapitulating the physiology of human organs in vitro [3–6]. Such organs-on-chips can be used for disease modeling and drug testing [4, 7, 8]. Moreover, microfluidic devices have been used extensively for studying cancer metastasis, tumor growth, and their interaction with other cells [1, 9, 10]. Such 'Tumor-on-chips' have proved their potential in drug screening applications [11, 12].

Unfortunately, the majority of such microfluidic devices remain limited to the research labs because of the tedious fabrication technique. Presently, such microfluidic devices are being fabricated by soft lithography and PDMS. Soft lithography uses masters manufactured with high-resolution photolithography, which has demonstrated the replication of micro to nano-level features [13–16]. However, soft lithography requires a cleanroom facility for masters fabrication, significant prior experience, and time-consuming fabrication steps, which hinder the application of PDMS microfluidic devices in a clinical setting. Moreover, two of the major parameters associated with soft-lithography: (1) expensive cleanroom setup cost and (2) non-compatibility with mass production make the per-unit cost of microfluidic devices on the higher side, preventing their commercialization.

3D printing has come out as a promising alternative to overcome the 'fabrication barrier' associated with microfluidic devices by enabling low-cost, rapid, one-step, and truly 3-dimensional fabrication of microfluidic devices [17–19].

✉ Subha N. Rath
subharath@bme.iith.ac.in

[1] Regenerative Medicine and Stem Cells Laboratory, Department of Biomedical Engineering, Indian Institute of Technology Hyderabad, Kandi, Telangana 502285, India

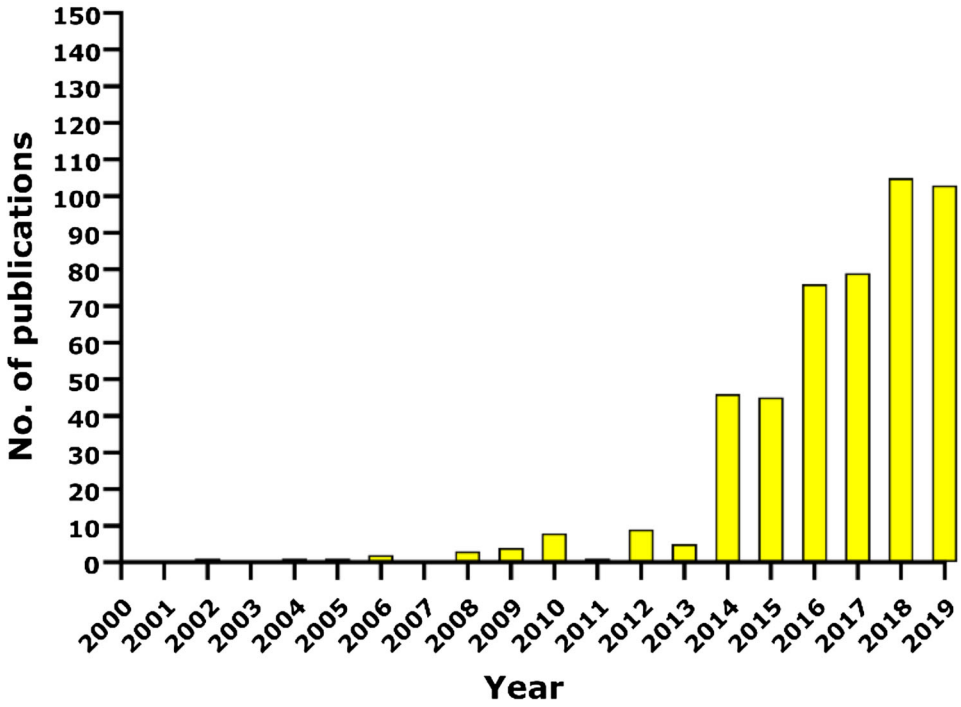

Fig. 1 Year-wise published papers with the keywords '3D printing' AND 'Microfluidics' (PubMed)

Unlike soft lithography, 3D printing fabricates microfluidic devices using a single machine, making it 'one-step' fabrication technology. Moreover, soft lithography is limited to planar 2-dimensional complexities, whereas 3D printing can quickly fabricate 'truly 3-dimensional' features such as crossover (overhanging) features. The popularity of 3D printing has been rising in the field of microfluidics because of the unprecedented fabrication ability. As shown in Fig. 1, the number of publications with the keywords '3D printing' AND 'Microfluidics' has been increasing swiftly for the last six years.

Stereolithography (SLA), extrusion-based technology, and inkjet 3D printing are three of the widely used technologies owing to their accessibility and affordability. Therefore, we have considered these three technologies in this review. Four fundamental manufacturing approaches can be used to fabricate microfluidic devices with the previously mentioned 3D printing technologies. Four fundamental manufacturing approaches can be classified as (1) direct printing approach, (2) mold-based approach, (3) modular approach, and (4) hybrid approach. Moreover, they can be further classified under each 3D printing technology, as shown in Fig. 2.

Previous articles have provided a detailed review of various 3D printing technologies and their applications for fabricating microfluidic devices [18, 20–22]. Moreover, Folch's laboratory focused particularly on FDM, SLA, and inkjet 3D printing technologies used for fabricating microfluidic devices [17]. Weisgrab et al. focused on integrating active elements such as sensors, valves, pumps, and actuators with 3D printed microfluidic devices [23]. Waldbaur et al. discussed 'direct one-step fabrication' methods, namely 3D printing from a perspective of materials [24]. Chan et al. focused on 3D printed diagnostic devices (point-of-care testing) [25]. However, no review is currently available focused on four fundamental 3D printing manufacturing approaches and implications of 3D printed microfluidics on the various fields related to healthcare, such as in vitro disease modeling and organ modeling, novel drug development, personalized treatment for cancer, and cancer drug screening. In this review, we first define four fundamental manufacturing approaches. Next, we discuss various applications of 3D printing manufacturing approaches for fabricating microfluidic devices, followed by the critical challenges related to 3D printing of microfluidic devices. Along with reported solutions to some of these challenges, we highlight research gaps associated with 3D printed microfluidics. Finally, we discuss possible implications of 3D printed microfluidic devices on the various fields of healthcare. Particularly, we discuss the role of multi-material 3D printing in the rapid development of biologically relevant 'organ-on-a-chip' models in the future. Such 3D printed organ-on-chips will be useful in disease modeling, organ modeling, and novel drug development. Besides, we discuss 3D printing's role in presenting various physical (matrix stiffness, topography, porosity) and chemical cues (material chemistry, cell adhesive ligands, and various growth factors) for guided differentiation of stem cells in the microfluidic devices. Molecular pathways involved in sensing matrix stiffness and chemical signals have been outlined. Finally, we review the recent progress in 3D printed 'tumor-on-chips' and 3D printing's ability to

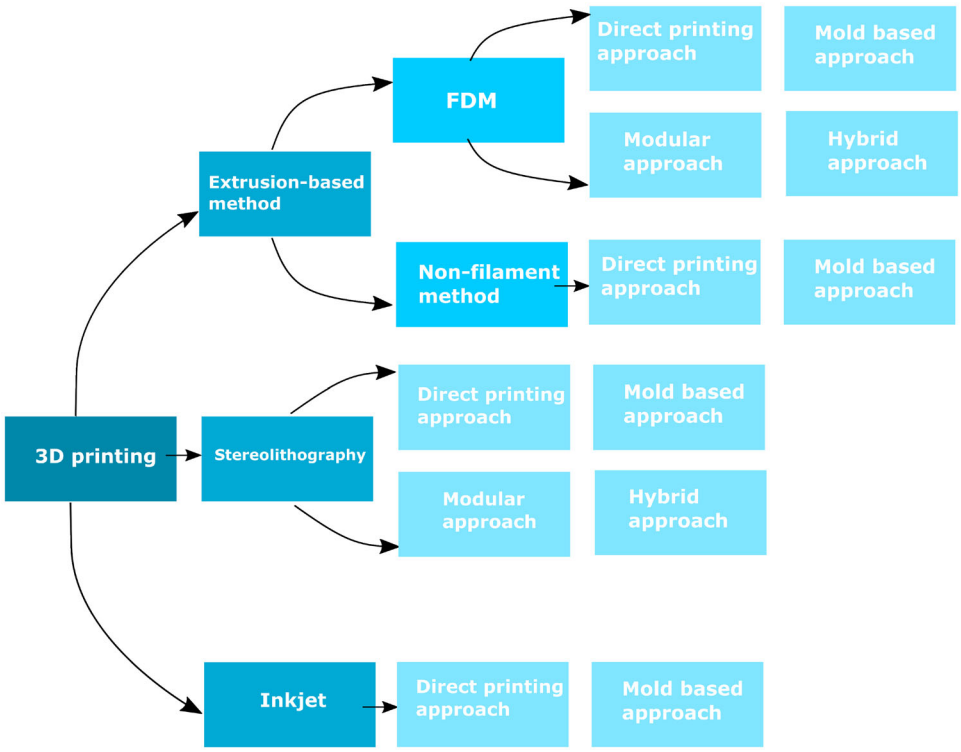

Fig. 2 Classification of four fundamental manufacturing approaches under each 3D printing technology

bring about a revolutionary change in healthcare by enabling rapid testing of drug efficacy and personalized treatment for cancer in the clinical settings. We conclude the review by highlighting future research directions in the field of 3D printed microfluidics.

Four fundamental manufacturing approaches

Direct printing approach

The direct printing method has been used widely to fabricate microfluidic devices [26–28]. Moreover, it is the fastest method among the four approaches for fabricating microfluidic devices. The direct printing method refers to the 'one-step' fabrication approach wherein the microfluidic devices are printed by incorporating microchannels, valves, inlets, and outlets without any assembly or bonding step (Fig. 3a). However, the device may undergo some post-processing steps for improving optical transparency, overall roughness, and biocompatibility.

Mold-based approach

Mold-based approach uses two kinds of molds: (1) sacrificial molds and (2) non-sacrificial molds. The mold-based method is an indirect 3D printing approach for fabricating microfluidic devices based on three steps. The procedure usually involves 3D printing of soft lithography molds and subsequent replica molding out of photocurable or thermally curable materials. If the molds are non-sacrificial, the last step requires bonding replica molded devices with either PDMS or glass slide using a conventional plasma treatment method. On the contrary, in sacrificial molds, the last step is mold removal by the dissolution of sacrificial materials. The sacrificial molds can be used only for one time, whereas non-sacrificial molds can be reused again. Mold-based method has been employed to overcome some of the limitations with a direct printing approach such as low optical transparency, cytotoxicity, and gas impermeability. 3D printed mold-based approach drastically reduces the time for fabricating the devices as it does not require multiple steps for fabricating the masters, unlike soft lithography. Figure 3b shows the non-sacrificial mold-based approach illustrating replica molding and bonding procedure.

Modular approach

The modular microfluidic devices are also known as 'Lego®-like' microfluidic devices. Similar to the Lego® models, this approach uses discrete microfluidic units such as L junction, T junction, mixer modules, straight channel modules, and reaction chambers, which can be assembled to make fully functional microfluidic devices (Fig. 3c) [29–31]. Unlike the traditional fabrication approach, the modular approach pro-

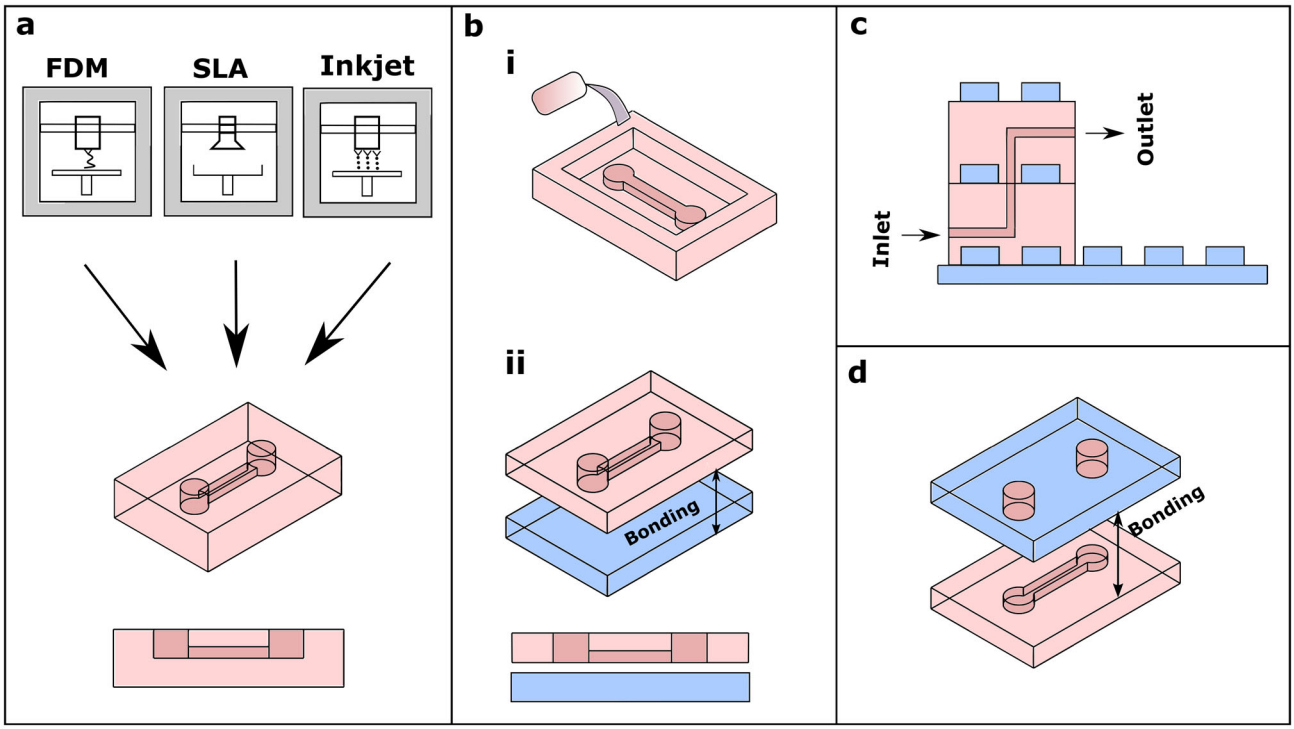

Fig. 3 Schematic illustration of four fundamental manufacturing approaches (**a**) direct printing approach showing fabrication of microfluidic devices with integrated inlets, outlets, and microchannels, (**b**) Non-sacrificial mold-based approach: (i) replica molding process with 3D printed molds (ii) sealing of channel with PDMS or glass slide from the bottom, (**c**) modular approach with 3D printed microfluidic modules assembled similar to Lego® blocks concept, (**d**) hybrid approach showing a 3D printed microchannel lower layer bonded with the upper transparent layer

vides the advantage of rapidly modifying the microfluidic chips by assembling individual units in a different configuration without fabricating a new device. The early modular approach was based on connecting different microfluidics modules using tubes and connectors [32, 33]. With the ease of manufacturing provided by 3D printing, now it is possible to fabricate microfluidic modules integrated with the connectors to enable rapid and effortless assembly [29, 34, 35].

Hybrid approach

The hybrid approach combines 3D printed microfluidic devices with other thermoplastic polymers or PDMS to overcome some of the limitations of the direct printing approach, namely low optical transparency and gas impermeability [36–38]. Moreover, a hybrid approach combines the benefits of both the PDMS and hard polymers in one microfluidic device, overcoming the limitations associated with 'all-polymer' and 'all-PDMS' devices. For example, polymers in hybrid microfluidic devices can minimize water evaporation and non-specific protein absorption associated with all-PDMS devices [39, 40]. Similarly, flexible materials like PDMS in hybrid devices allow control of fluid flow using microvalves and the application of mechanical stimulation, which cannot be effectively achieved with all-polymer microfluidic devices. Figure 3d shows the schematic illustration of a hybrid approach with upper transparent material with inlets and outlets being bonded to a lower 3D printed channel device to fabricate a hybrid microfluidic device.

Extrusion-based 3D printing

Extrusion-based approach can be classified into two types (1) filament based: fused deposition modeling (FDM), (2) non-filament-based extrusion approach. FDM was first introduced in 1988 by S.Scott Crump, the co-founder of Stratasys [41]. FDM processes filament form of the polymers, whereas the non-filament-based extrusion method processes pellets, powder, and various hydrogels.

FDM-based technique drives the thermoplastic polymer filaments toward the extruder head, where the temperature is maintained above the polymer's melting point. The extruded molten thermoplastic material rapidly solidifies at room tem-

perature and gets deposited on the build platform layer by layer.

In 2002, the first non-filament-based extrusion system was introduced, known as '3D-Bioplotter' [42]. Such systems dispense materials by using a pneumatic system or motor system through a nozzle. A motor-based extrusion system is further classified in the screw-driven mechanism and piston-driven mechanism. Usually, motor-driven systems are used for printing higher viscosity materials with accurate control over the extrusion amount of the material compared to the non-motor based systems [42–44]. However, a higher number of moving parts in a motor-based extrusion system is a disadvantage. Moreover, non-filament-based extruders are equipped with the heating (and cooling) elements to print with pellet and powder forms of materials and thermoresponsive materials.

Microfluidic devices fabricated by FDM: direct printing approach

Two of the main features which make FDM an attractive technology for the fabrication of microfluidic devices are (1) wide range of biocompatible thermoplastic polymers for 3D printing such as polyethylene terephthalate glycol (PETg), polylactic acid (PLA), polycarbonate (PC), cyclic olefin copolymer (COC), thermoplastic polyurethane (TPU), polymethylmethacrylate (PMMA), polypropylene (PP), and acrylonitrile butadiene styrene (ABS), (2) affordability and accessibility of FDM printers and materials.

Bruce Gale's group demonstrated 3D printed flexible microfluidic devices from TPU with channel sizes ranging from 50 to 400 μm [28]. They found TPU was compatible with several organic solvents except for acetone and chloroform. Moreover, TPU was found optically transparent as well as biocompatible when mIMCD3 cells were cultured on them. Direct printing with FDM includes a bridging layer to seal the microchannels. Sagging of the polymers is often observed in this bridging layer, leading to channel blockage and impacting the channel visibility. Bruce Gale's group demonstrated practical solutions to prevent sagging of polymers by changing the channels' geometry from rectangular or square to ellipsoid, triangular, and diamond shape to minimize the bridging gap.

Apart from TPU, hard thermoplastic materials such as transparent PLA and PETg have been used to fabricate transparent microfluidic devices for droplet formation, DNA melting characterization, and mixing application [45]. Figure 4a shows a 3D printed serpentine mixer made from PETg filament.

FDM 3D printing allows the integration of porous membranes, glass coverslips, and liquid reagents during the printing process, which opens a myriad of applications.

Leroy Cronin's group has demonstrated the ability to incorporate reagents while 3D printing the 'reactionware' devices using polypropylene material [46]. They have also demonstrated the fabrication of intricate reactionware devices for chemical synthesis (Fig. 4b), including gold nanoparticles synthesis [47]. Po Ki Yuen demonstrated a process for the embedding of porous cellular acetate membrane in between two 3D printed open serpentine channels, which can be used for continuous perfusion cell culture (Fig. 4c(i–iv)) [48]. Moreover, for better optical transparency, he successfully embedded glass coverslips during the printing process of a serpentine channel (Fig. 4d).

Gaal et al. integrated thin materials such as wires, glass, and electrodes into the 3D printed microchannels made of PLA [49]. They demonstrated the fabrication of an electronic tongue sensor by embedding flexible interdigitated electrodes during the printing process.

Li et al. used multi-material FDM 3D printing to integrate membrane made out of composite lay-felt filament in ABS microfluidic device for colorimetric determination of nitrate in the soil (Fig. 4e–f) [50]. Recently, PLA-based microfluidic devices were used for fabricating core–shell metallic nanoparticles [51].

Salentijn et al. carried out extensive research on the characterization of biocompatibility, solvent compatibility, and autofluorescence of various FDM polymers available for 3D printing [52]. They have studied the effect of shell number and infill density on leakage of the devices. Although 100% infill density is recommended to prevent fluid leakage during high-pressure fluid flow, they reported 20% infill density with four walls around channels prevented fluid leakage.

FDM 3D printing enables the fabrication of scaffolds for more efficient enzyme immobilization with high specific surface area and surface activation groups. Such 3D printed scaffolds were chemically modified and integrated into microfluidic devices for continuous reactions [53].

Microfluidic devices fabricated by FDM: mold-based approach

Both sacrificial and non-sacrificial molds can be fabricated by fused deposition modeling. For making sacrificial molds, polyvinyl alcohol (PVA) and acrylonitrile butadiene styrene (ABS) have been used widely as they can be easily dissolved in water and acetone, respectively. Moreover, PLA- and ABS-based non-sacrificial molds have also been reported for fabricating microfluidic devices.

ABS-based sacrificial molds

Saggiomo et al. demonstrated the fabrication of various microfluidic devices, such as intricate spiral channels (Fig. 5a(i, iii)), channels with varying diameters (Fig. 5a(ii)),

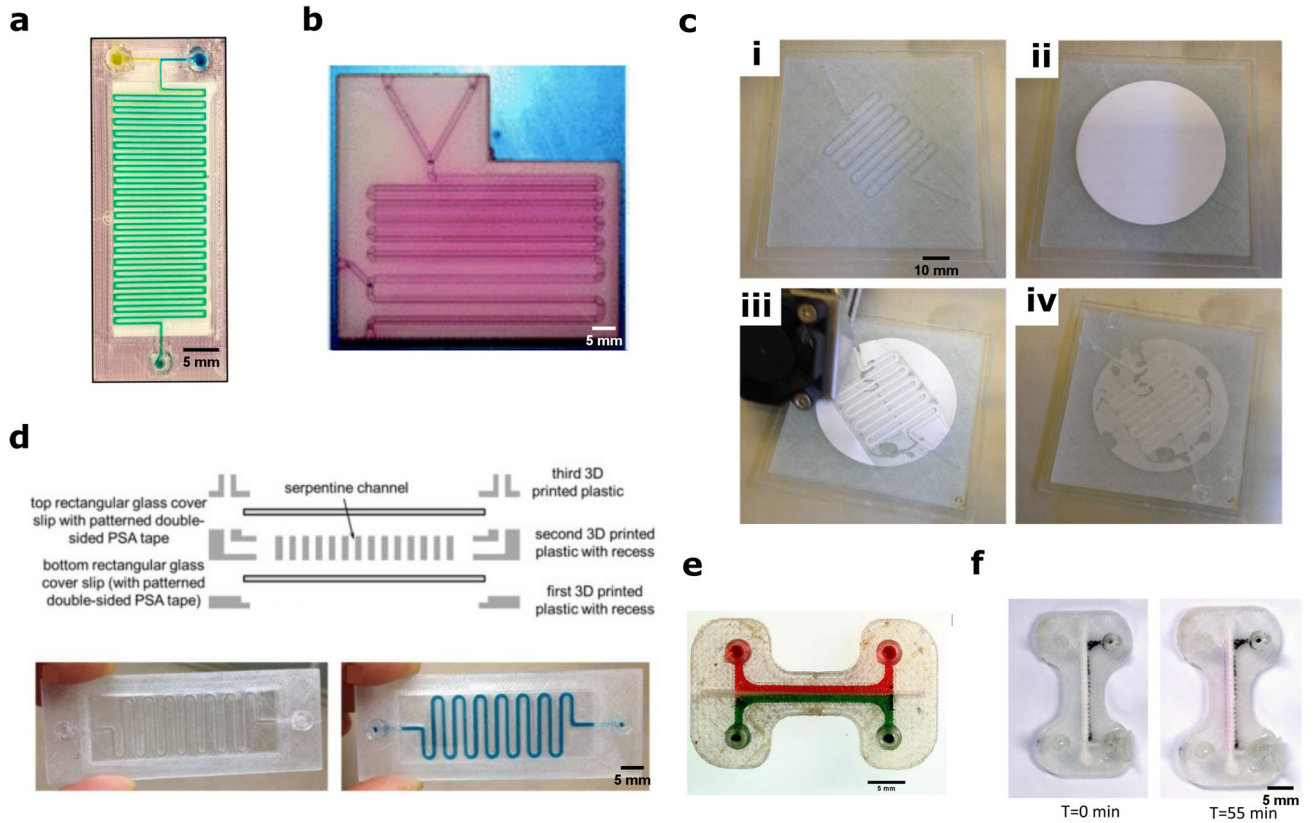

Fig. 4 Microfluidic devices fabricated using the FDM–direct printing approach (**a**) a 3D printed serpentine mixer from PETg filament, (**b**) a reactionware device for chemical synthesis fabricated by FDM, (**c**) process of integrating cellular acetate membrane during 3D printing: (i) 3D printing of lower half of the serpentine channel, (ii) the cellular acetate membrane is glued to the printed channel by pausing the 3D printer, (iii) 3D printing is resumed for printing the upper half of the serpentine channel, and (iv) final serpentine channel with the embedded membrane, (**d**) 3D printed serpentine channel with integrated coverslips, (**e**) 3D printed device with the lay-felt membrane in the middle separating the two chambers, (**f**) device for colorimetric detection of nitrate in the soil: soil mixed with zinc dust and $CaSO_4$ is introduced in the right channel, and Griess reagent is injected in the left channel. Panel (**a**) is reprinted with permission from [45]. Copyright 2018 American Chemical Society. A scale bar has been added based on channel size reported. Panel (**b**) is reproduced from Ref. [47] with permission from The Royal Society of Chemistry. A scale bar has been added based on overall dimensions reported. Panels (**c**) and (**d**) are reprinted from [48], with the permission of AIP Publishing. A scale bar has been added in (**c**) and (**d**) based on channel size reported. Panels (**e**) and (**f**) are reprinted with permission from [50]. Copyright 2018 American Chemical Society. A scale bar has been added in (**f**) based on overall dimensions reported

and Hilbert cube (Fig. 5a(iv)) using ABS sacrificial molds and PDMS replica molding [54]. Moreover, they have also shown the integration of various electronic components during PDMS replica molding, such as UV LED light for fluorescence detection, nichrome resistance wire for selective heating, copper wire allowing high-resolution NMR spectroscopy, and Arduino microcontroller for RGB color sensing application.

Tang et al. integrated laser-cut stainless steel pieces with 3D printer nozzles to fabricate microfluidic channels with unconventional shapes such as semielliptical and triangular cross sections [55]. They poured uncured PDMS after placing the molds on a 5-mm-thick cured PDMS block to eliminate the bonding procedure for sealing the channels.

PVA-based sacrificial molds

Hashimoto's group demonstrated a method to fabricate microfluidic channels from PVA sacrificial molds, as shown in Fig. 5b(i–v) [56]. They fabricated T channels for forming water in oil droplets, straight microchannels for the dynamic culture of endothelial cells, microfluidic devices with 3D interconnections using modular sacrificial molds, and 3D herringbone chaotic mixer using PVA molds and PDMS replica molding. Apart from the replica molding out of PDMS, they have also shown replica molding from UV curable hydrogels such as poly(ethylene glycol) diacrylate (PEGDA) and heat-curable hydrogels such as gelatin. They reported two significant limitations with the fabrication of microfluidic devices from PVA 3D printed molds. First, the molds may become flaccid with five minutes of exposure

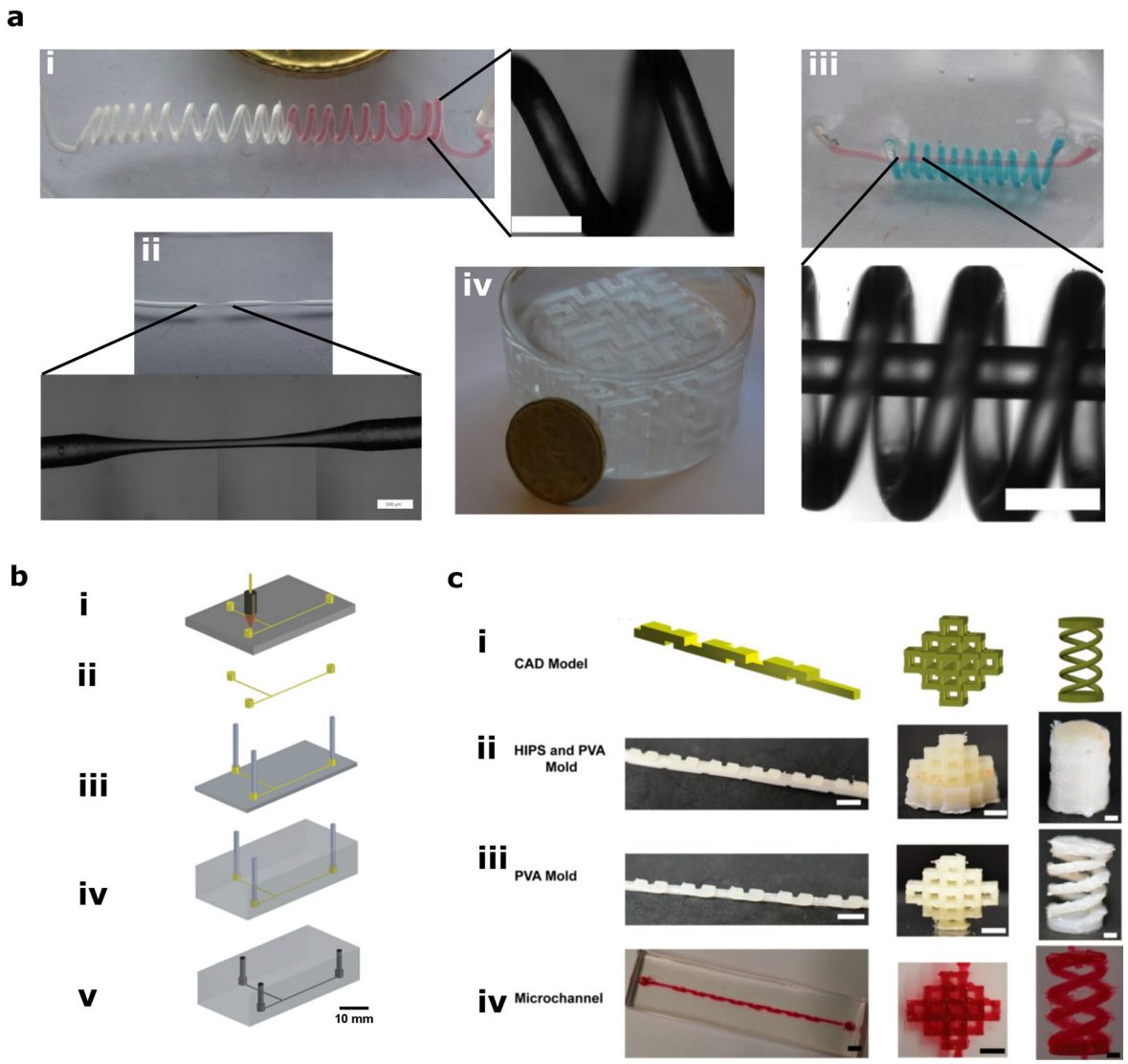

Fig. 5 Microfluidic devices fabricated with the FDM–mold-based approach (**a**) microfluidic channels fabricated by ABS sacrificial molds: (i) spiral microchannel (scale bar = 1 mm), (ii) microchannel with variable diameters, (iii) spiral microchannel wrapped around a straight microchannel (scale bar = 1 mm), (iv) Hilbert cube. (**b**) Step-by-step procedure of fabricating microfluidic devices from PVA sacrificial molds: (i) 3D printing of PVA mold, (ii) removal of mold from the printing bed, (iii) placement of mold on cured polymer matrix with PTFE tubes inserted in inlet and outlet sockets, (iv) casting with an uncured polymer, (v) mold removal with water, (**c**) dual-sacrificial material mold-based technique: (i) CAD models of the serpentine microchannel (left), pyramid network (middle), and dual helix channel (right), (ii) printed microchannels with PVA and HIPS material, (iii) after removing the HIPS, revealing the PVA molds, (iv) after replica molding with PDMS and removal of PVA. Scale bar for (**c**): 3 mm for left panel, 2.5 mm for middle panel, and 2 mm for the right panel. Panel (**a**) is reproduced from [54] under the Creative Commons Attribution 4.0 International Public License (https://creativecommons.org/licenses/by/4.0/). Panel (**b**) is reproduced from [56] with permission of John Wiley and Sons. A scale bar has been added based on channel size reported. Panel (**c**) is reproduced from [57] under the Creative Commons Attribution 4.0 International Public License (https://creativecommons.org/licenses/by/4.0)

to ambient air because of the hygroscopic nature of PVA. Second, the excessive time requirement to dissolve PVA molds with larger size and complexity. Due to hygroscopic nature, it is recommended to keep the filament and the molds in airtight containers with desiccant packs to protect them from the moisture. The same group devised a method to fabricate microfluidic device molds with overhanging or helical features with dual material printing using high impact polystyrene (HIPS) and PVA [57]. In this method, HIPS is used as a support material for 3D printing overhanging features out of PVA (Fig. 5c(i, ii)). HIPS is later removed by submerging the molds in limonene to revel the PVA structure (Fig. 5c(iii)). Lastly, the PVA molds are used for replica

molding out of PDMS and subsequently removed by dissolution in water (Fig. 5c(iv)).

Non-sacrificial molds

Salentijn et al. used 3D printed PLA non-sacrificial molds for fabricating microfluidic channels out of PDMS [52]. These microfluidic devices were sealed with another PDMS block using plasma treatment. However, it was challenging to seal PDMS devices with plasma treatment due to the high surface roughness transferred to a PDMS bonding surface from FDM molds. To address the roughness problem, Po Ki Yuen printed soft lithography molds on embedded glass coverslips, which produced a smooth PDMS bonding surface and allowed successful sealing with another PDMS block or glass coverslip [48].

Shankles et al. used 3D printed ABS molds to fabricate droplet generators, gradient generators, and 3D crossover features designed in custom-made software. The software gives a list of parameterized microfluidic features and has an integrated slicer program to produce g codes [58]. In the fabrication procedure, they have incorporated the polishing of ABS surface with acetone at 50 °C, which significantly reduced the surface roughness of the molds.

Microfluidic devices fabricated by FDM: modular approach

Morgan et al. used transparent PLA filament to fabricate droplet forming devices, dental pulp stem cells encapsulation devices, and modular lego®-like devices [59]. They have designed various fluidic modules such as T junction, flow-focusing junction, and mixing module, which can be assembled like Lego® blocks (Fig. 6a). Due to the O-ring placed between male and female fluidic blocks, pressure up to 2000 kPa could be sustained, which exceeded the pressure tolerance of the devices fabricated by PDMS. They have designed a modular system comprised of seven different fluidic elements for droplets production, as shown in Fig. 6b.

Tsuda et al. also used PLA to fabricate droplet generators, bacterial cells encapsulation devices, PDMS membrane integrated valves (flow selector device), and modular devices [60]. FDM modular devices with high surface roughness and rigid thermoplastic polymers can cause leakage from the interconnections. Tsuda et al. used chemical treatment with dichloromethane (DCM) vapor for 15 min to reduce surface roughness and prevent any leakage from the interconnections of the fluidic modules. In addition to chemical treatment, the PTFE tape can be wrapped around male connectors to prevent further leakage. They have fabricated a leak-proof modular droplet generator device by assembling two single input channel modules, a serpentine mixing module, and a droplet generator module, as shown in Fig. 6c.

Nie et al. fabricated open-channel Lego®-like fluidic blocks from PLA material [61]. The device operated on the principle of capillary driven fluid flow, which reduced the chances of leakage from the interconnections as no external pumping was required. Moreover, the channels need not be fabricated inside the microfluidic modules because of the open and capillary driven system. They have designed several fluidic modules, which can be assembled for gradient generation, dynamic perfusion-assisted bone scaffold degradation, and dynamic culture of cells.

Microfluidic devices fabricated by non-filament method: direct printing approach

Ching et al. developed a novel method involving 3D printing of the outline of microchannels on flat PMMA substrates [62]. The printed outline of the channels got sealed with another PMMA substrate from the top with mechanical fasteners and spacers for controlling the overall width of the channels (Fig. 7a(i–iii)). Using this approach, they fabricated various microfluidic devices such as a serpentine mixer, droplet generator, Y channel, and air–liquid interface cell culture device. Some of these devices are shown in Fig. 7b(i–v). They also demonstrated variable size droplet generator and fluidic valves with localized deformation of the microchannels. Moreover, integration with electrical components was also shown by printing the channels directly on the printed circuit boards (PCB).

Moreover, the non-filament direct printing approach has also been used for fabricating liver-on-a-chip [39] and nervous system-on-a-chip [63] from polycaprolactone (PCL).

Microfluidic devices fabricated by non-filament method: mold-based approach

Non-filament-based method usually employs a sacrificial mold-based approach for fabricating microfluidic devices. Materials such as wax, sugar, pluronic, and agarose have been successfully 3D printed for fabricating sacrificial molds, as discussed below.

Wax-based sacrificial molds

Jennifer Lewis' group used paraffin organic material for fabricating sacrificial molds for interconnected 3D mixing units [64]. The sacrificial paraffin ink was dissolved by heating at 60° C, thereby exposing the interconnected microfluidic network embedded in the epoxy resin.

Toohey et al. used a sacrificial ink made of 60% petroleum jelly and 40% microcrystalline wax to fabricate microvascular networks embedded in the epoxy resin [65]. This microvascular network was capable of self-healing the cracks, mimicking the human skin.

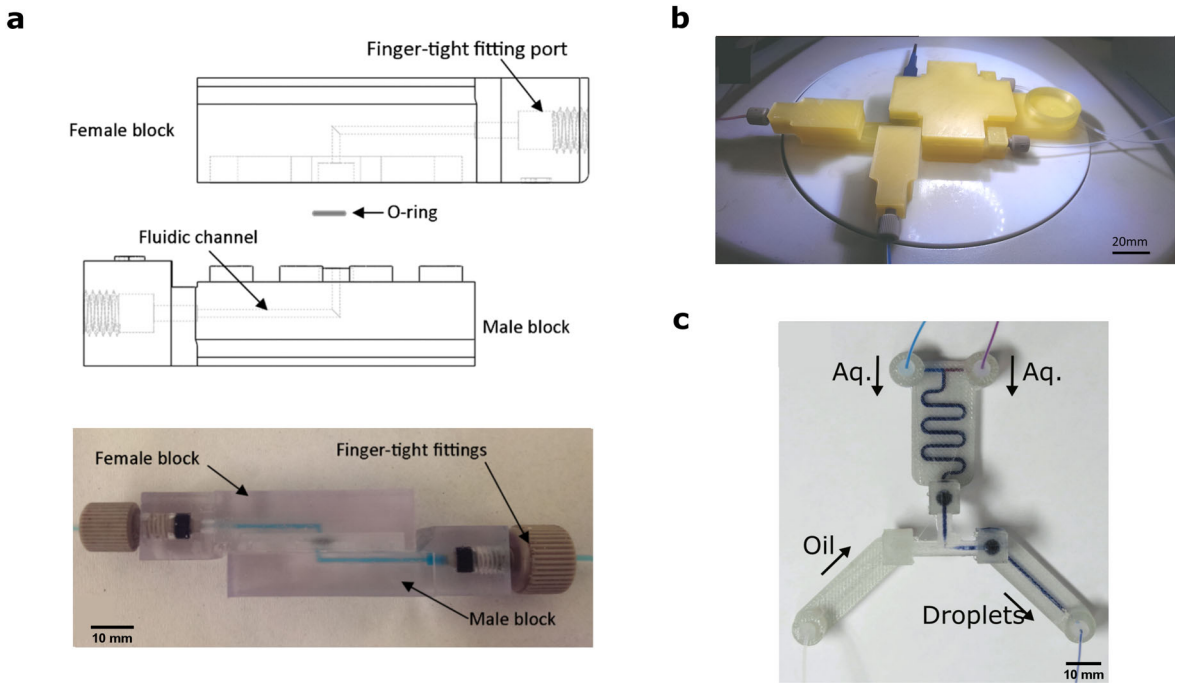

Fig. 6 Microfluidic devices fabricated with the FDM–modular approach (**a**) male and female microfluidic modules, (**b**) a modular system with seven different elements for droplet production, (**c**) a droplet generator device assembled with two single input channel modules, one serpentine mixer module, and one flow-focusing module. Panels (**a**) and (**b**) are reproduced from [59] under the Creative Commons Attribution 4.0 International Public License (https://creativecommons.org/licenses/by/4.0/). A scale bar has been added in (**a**) based on overall dimensions reported. Panel (**c**) is reproduced from [60] under the Creative Commons Attribution 4.0 International Public License (https://creativecommons.org/licenses/by/4.0. A scale bar has been added based on channel size reported

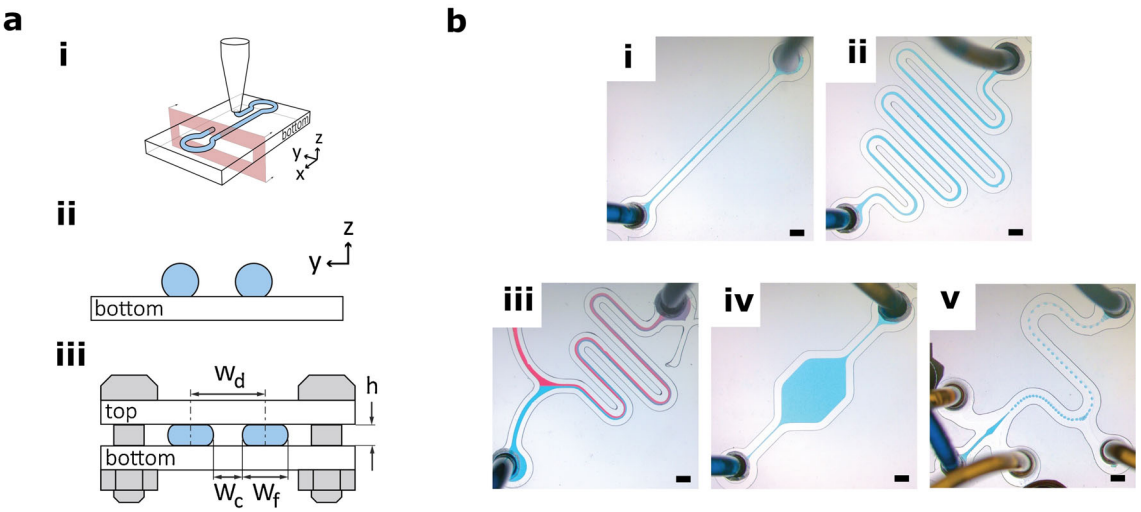

Fig. 7 Microfluidic devices fabricated with non-filament method–direct printing approach (**a**) process of printing the microfluidic device: (i) 3D printing of outline of the microchannel on PMMA substrate, (ii) front view of the printed microchannel, (iii) the microchannel is sealed with upper PMMA substrate and mechanical fasteners (h = gap between to PMMA substrates, W_f = Width of one filament, W_d = Width in CAD drawing, W_c = Actual width of the channel). (**b**) Various microchannels formed with this method: (i) a straight microchannel, (ii) a serpentine mixer, (iii) Y channel with serpentine mixing channel, (iv) a chamber, (v) a flow-focusing droplet generator. Scale bar for (**b**) = 1 mm. Panels (**a**) and (**b**) are reprinted from [62] Copyright 2019, with permission from Elsevier

Sugar-based sacrificial molds

He et al. compared the properties of different sugars, namely proper printing temperature, properties during fusion, and fabrication cost to select an ideal sugar for 3D printing [66]. They selected maltitol sugar because of its stable nature during the melting process and better flow properties during the extrusion. The procedure for the fabrication of microchannels involves eight steps: (1) pouring of PDMS on glass/polymer substrate to form the base layer, (2) printing of sugar microchannels using hot melt extruder at 150 °C, (3) extrusion of PDMS as a support material to prevent sugar structures from collapsing, (4) curing the PDMS at 100 °C for 5 min, (5) printing of the next layer of sugar on the support layer, (6) repetition of the whole process until the desired structure is printed, (7) pouring and curing of PDMS to embed the whole structure, and (8) heating the microchannel structure in boiling water at 100° C for 10 min to dissolve the sugar.

Miller et al. 3D printed carbohydrate glass consisting of a mixture of glucose, sucrose, and dextran at 110° C to form microvascular networks embedded in the cell encapsulated photocurable hydrogel matrix [67]. The carbohydrate mixture can be eventually washed away in a cell culture medium to form a perfusable network. 3D printable mixture of glucose, sucrose, and dextran demonstrated a mechanically stiff nature at room temperature, excellent printability, optical transparency, and compatibility with the photopolymer matrix. They have derived a mathematical relationship between the diameter of the filament and the nozzle travel speed as mentioned below,

$$D(v) = \frac{A}{\sqrt{v}} \tag{1}$$

where D = diameter of filament, v = nozzle travel speed, A = constant based on nozzle diameter, and extrusion flow rate. According to the relationship, the diameter of printed carbohydrate glass filament varies inversely with the square root of the nozzle travel speed.

Gelber et al. 3D printed sugar alcohol (isomalt)-based sacrificial molds at 115° C embedded in the agarose [68]. The molds quickly dissolved in agarose hydrogel to reveal a combinatorial mixer generator, as shown in Fig. 8a.

Pluronic-based sacrificial molds

Lewis' group devised a novel omnidirectional 3D printing strategy, which does not print in a conventional layer-by-layer fashion [69]. In this method, a fugitive organic ink was printed inside a thermally or photocurable resin matrix, which physically supported the fugitive ink. They used pluronic F127 as fugitive organic ink, which could be liquefied below 4 °C temperature to reveal interconnected, truly three-dimensional microvascular networks.

In another study, Lewis' group used the same pluronic F127 as sacrificial material and cell-laden gelatin methacrylate (GelMA) as a matrix material to fabricate vascularized heterogeneous tissue constructs [70]. Figure 8b shows a heterogeneous tissue construct printed with a GelMA ink containing two different cells (green fluorescent protein-expressing HNDFs and non-fluorescent 10T1/2s) and a sacrificial pluronic ink, which was later endothelialized with RFP HUVECs.

Agarose-based sacrificial molds

Bertassoni et al. 3D printed sacrificial agarose fibers at 4° C, which were embedded into the photocurable hydrogel matrix for fabricating vascularized networks, as shown in Fig. 8c(i) [71]. As agarose fibers did not adhere to the matrix material, they were simply removed manually after the curing of matrix material instead of dissolving them at an elevated temperature (Fig. 8c(ii)).

Stereolithography

Chuck Hull developed stereolithography (SLA) in 1986, which typically uses a light source in the range of 380–405 nm wavelength to cure the photocurable resin formulations. The equipment consists of an XY scanning mirror, which deflects the light in a computer-generated pattern to cure specific regions of the resin layer. Once the layer is cured, the build platform moves away from the laser source (in case of inverted configuration) by a certain amount (set by layer height), leaving space for the next layer. More recently developed DLP (Digital light processing) technology uses a digital projector that projects a whole layer's image and cures it in one go, making the process faster than SLA [72].

Microfluidic devices fabricated by stereolithography: direct printing approach

Folch's group and Breadmore's group were few of the early researchers to demonstrate 3D printing of microfluidic devices with stereolithography.

Folch's laboratory used 3D systems' Viper SL printer and biocompatible WaterShed XC 11,122 resin to fabricate microfluidic devices [26]. Breadmore's group used a Miicraft printer for fabricating a 3D mixer, 3D gradient generator, droplet extractor, ITP separation device, and tapwater nitrate analysis device [27]. In stereolithography, removal of the trapped uncured resin from the channels controls the minimum achievable channel width. For example, Breadmore's group found that the channels with a width below

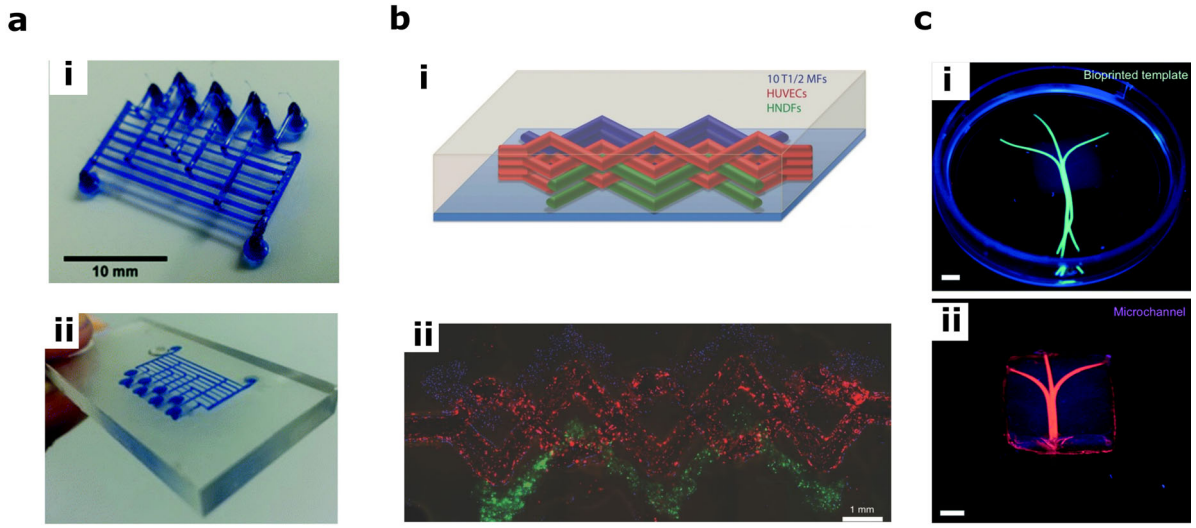

Fig. 8 Microfluidic devices fabricated with non-filament method–mold-based approach (**a**) sugar-based sacrificial molds: (i) 3D printed isomalt sacrificial template, (ii) a combinatorial mixer generator after casting with agarose (**b**) pluronic-based sacrificial molds: (i) Schematic of the heterogeneous tissue construct with semi-woven features, (ii) fluorescent image of the printed tissue construct (**c**) agarose-based sacrificial molds: (i) 3D printed agarose sacrificial template (green) encapsulated in GelMA matrix, (ii) removal of agarose fibers and subsequent perfusion with fluorescent microbead suspension (pink). Scale bar for (**c**) = 3 mm. Panel (**a**) is reproduced from Ref. [68] with permission from The Royal Society of Chemistry. Panel (**b**) is reproduced from [70] with permission of John Wiley and Sons. Panel (**c**) is reproduced from Ref. [71] with permission from The Royal Society of Chemistry

250 μm were clogged with uncured resin, making the minimum achievable channel width as 250 μm on the Miicraft printer.

Due to the unknown composition of proprietary resins, researchers are gradually moving toward in-house developed resins made from poly(ethylene glycol) diacrylate (PEG-DA) for fabricating the microfluidic devices with better resolution, optical transparency, and biocompatibility.

Folch's group used the ILIOS DLP 3D printer and PEG-DA-250 resin with the Irgacure-819 photoinitiator to fabricate transparent microfluidic devices [73]. They have shown that transparent resins can be effectively cured with 385 nm UV light, producing finer channel geometries with improved Z resolution. Moreover, they found the biocompatibility of 3D printed Petri dishes comparable with the standard tissue culture plates.

In another study, Folch's group used PEG-DA-258 resin with Irgacure-819 photoinitiator and isopropyl thioxanthone photosensitizer to improve the resolution and absorbance properties of PEG-DA resin [74]. They successfully fabricated 52 μm wide individual micromirror arrays, chaotic F mixer (Fig. 9a), 25-μm-thick membrane valve rotary mixer, and high-resolution capillary channels with 27 μm width (Single pixel width of printer's projector). Such high-resolution capillary channels act as capillary burst valves and effectively trap hydrogel inside the central channel, as shown in Fig. 9b [75].

Gong et al. demonstrated the smallest 3D printed microchannel having dimensions of 18 × 20 μm using a custom DLP printer and optimized resin formulation containing PEG-DA-258 [76].

Folch's group has also optimized absorbance properties of commercially available PDMS resin for 3D printing high-resolution PDMS microfluidic devices with a DLP printer [77]. They have demonstrated the fabrication of 500 μm wide channels from PDMS resin (Fig. 9c). Moreover, the optical transparency and biocompatibility of 3D printed PDMS parts were found to be the same as the molded PDMS (sylgard-184) parts.

Au et al. demonstrated 3D printing of microfluidic devices integrating microvalves [78]. They fabricated a single-valve device by printing a 100-μm membrane-like layer, which can be deflected by air-pressure to control the fluid flow (Fig. 9d(i–iii)). They also fabricated a microfluidic device with four valves, which can stimulate cells with ATP solutions (Fig. 9d(iv, v)). Moreover, Rogers et al. also demonstrated the integration of valves with 3D printed microfluidic devices made from PEG-DA resin [79].

Researchers have also demonstrated SLA-based microfluidic droplet generators and nanoliposome generators [80, 81]. Recently, Chiado et al. have introduced active moieties like –COOH with photocurable resin for 3D printing microfluidic devices for the detection of cancer angiogenesis biomarkers like vascular endothelial growth factor (VEGF) and angiopoietin-2 (Ang-2) by a colorimetric immunoassay

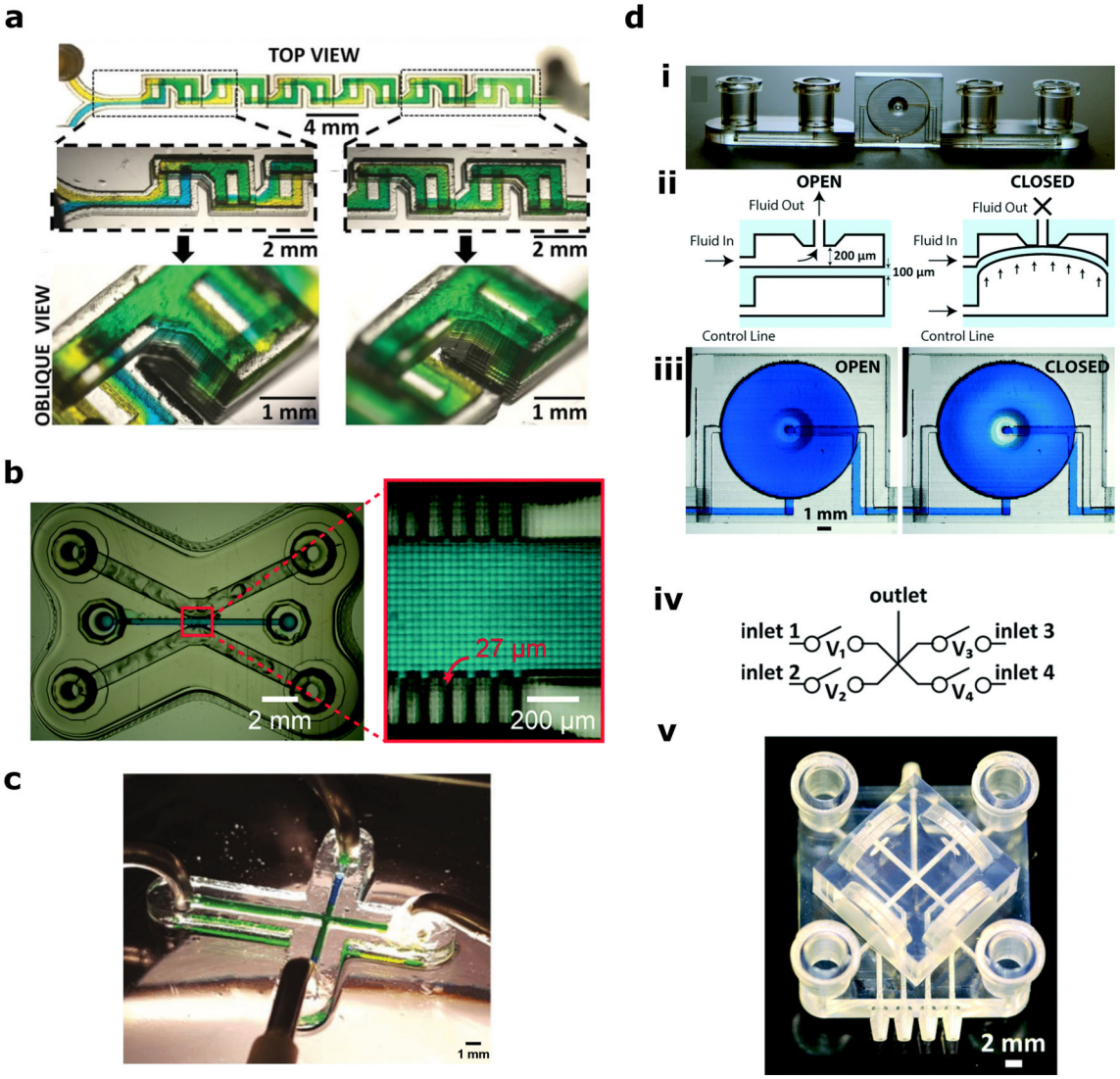

Fig. 9 Microfluidic devices fabricated with SLA- Direct printing approach (**a**) 3D printed chaotic F-mixer (**b**) a microfluidic device with 27 µm wide capillary microchannels trapping the blue dye in the central channel (**c**) a microfluidic device with 500 µm wide channels made from PDMS resin (**d**) integration of microvalves in 3D printed microfluidic devices: (i) a 3D printed single-valve device, (ii) schematic of a valve in the open (left) and closed (right) states, (iii) microvalve in the open (left) and closed (right) states visualized with blue dye, (iv) Circuit diagram of the four-valve device, (v) 3D printed four-valve device used for ATP stimulation. Panel (**a**) is reproduced from [74] with permission of John Wiley and Sons. Panel (**b**) is reproduced from Ref. [75] with permission from The Royal Society of Chemistry. Panel (**c**) is reproduced from [77] with permission of John Wiley and Sons. A scale bar has been added based on channel size reported. Panel (**d**) is reproduced from Ref. [78] with permission from The Royal Society of Chemistry

[82]. The carboxyl group captures biological elements with a primary amine in its structure and can be used in biosensing applications. Stereolithography has also been used for fabricating bioreactors for osteochondral tissue culture [8, 83], microfluidic devices for 3D cell culture [84], and devices for multicellular spheroid culture [85].

Microfluidic devices fabricated by stereolithography: mold-based approach

Stereolithography has been used widely for making non-sacrificial soft-lithography molds for PDMS microfluidic devices. The popularity of this approach is growing because of a similar concept to soft-lithography with lesser and simplified fabrication steps.

Fabrication of PDMS microfluidic devices out of SLA molds consists of four steps: (1) 3D printing of molds, (2)

post-processing of molds, (3) replica molding, and (4) bonding. Post-processing is usually required to prevent PDMS from adhering to the mold surface, facilitate curing of PDMS, and remove residual resin monomers and catalysts found on the surface of the molds [19]. Researchers have optimized these post-processing steps, including washing uncured resin, UV post-curing, heating, and silanization. Although the overall post-processing steps remain the same, treatment time and heating temperature often vary with each proprietary resin.

Chan et al. suggested heating the molds at 130 °C to remove any uncured resin residuals and silanization to inhibit PDMS from adhering to the mold surface [19]. They have demonstrated the replica molding of complex overhanging features by optimizing peeling direction and post-processing steps.

As acrylate-based resins do not allow PDMS curing, time-consuming post-processing steps such as sonication with ethanol and ink airbrushing are often required [86]. To overcome limitations related to acrylate-based resins, Bazaz et al. used methacrylate-based resins, which did not need any post-fabrication steps [87].

Moreover, this approach has also been used to fabricate microfluidic devices studying the interaction between leukocytes and TNFα-activated endothelial cells [88] and multi-depth droplet generators capable of controlling the shape of droplets [89].

Microfluidic devices fabricated by stereolithography: modular approach

Bhargava et al. fabricated various microfluidic modules such as fluidic junction modules, mixer module, and straight channel module using SLA 3D printer and WaterShed XC 11,122 resin [29]. These modules were connected to generate microdroplets and to mix fluids with a tunable mixing ratio.

Recently, Ching et al. demonstrated SL printed 3D microfluidic networks, discretized in various subunits to overcome channel blockage due to trapped resin [90].

Vittayarukskul et al. used 3D printed molds for making 2 × 2 Lego® blocks with microchannels, which can be stacked to create 3D microfluidic devices [35]. They reported a very low burst pressure of 0.11–0.13 psi because of the high surface roughness of the molds. On the contrary, Po ki Yuen reported a robust interconnection system which can sustain fluid pressure up to 51.1 psi [34]. He introduced a SmartBuild system consisting of a motherboard on which various microfluidic components such as mixing chambers and reaction chambers can be assembled.

Inkjet 3D printing

There are two types of inkjet 3D printing: (1) photopolymer-based and (2) powder-based. Photopolymer-based inkjet printing uses liquid acrylate-based photopolymers, which are cured layer-by-layer with UV light. Unlike stereolithography, this technology uses a computer-assisted array of inkjet heads that dispense liquid photopolymers precisely [91]. Photopolymer-based inkjet printing is commercially known by two different names, namely multijet and polyjet. Polyjet is a proprietary technology of Stratasys commercialized by Objet in 1999 [92]. On the other hand, multijet printing was commercialized by 3D systems in 1996 [93]. Although the working principle of both technologies is the same, the support material differentiates the two technologies. In the case of polyjet, the support material is a combination of acrylic monomer, polyethylene, propylene, and glycerin, which need to be removed by high-pressure waterjet, whereas in multijet, the support material is wax, which can be melted away in the oven after printing [92].

The powder-based inkjet 3D printing is also known as the binder jetting process. In the binder jetting process, the printing head delivers droplets of binding material on a powder bed, which selectively binds the material to build an object layer-by-layer. This technology mainly uses ceramics and metallic powders, limiting its application to fabricate polymer-based microfluidics.

Microfluidic devices fabricated by inkjet 3D printing: direct printing approach

Inkjet technology has been used to fabricate complex mixing devices such as caterpillar mixer (Fig. 10a(i)), Tesla mixer (Fig. 10a(ii)), and HC mixer (Fig. 10a(iii)) [94]. Anderson et al. used inkjet 3D printing to fabricate microfluidic devices integrated with porous membranes to study drug transport and the effect of the same on cultured cells [95].

Recently, inkjet 3D printing was used to fabricate microfluidic devices to collect micro/nanoparticles from a sample by free-flow electrophoresis. The device was also capable of collecting exosomes from a biological sample [96].

One of the significant benefits of this technology is 'multi-material printing,' capable of fabricating microfluidic devices with a combination of rigid and flexible materials. Ji et al. integrated flexible and rigid materials in an emulsion generator device (Fig. 10b(i, ii)) [97]. A flexible channel in the emulsion generator can be deformed with a pneumatic

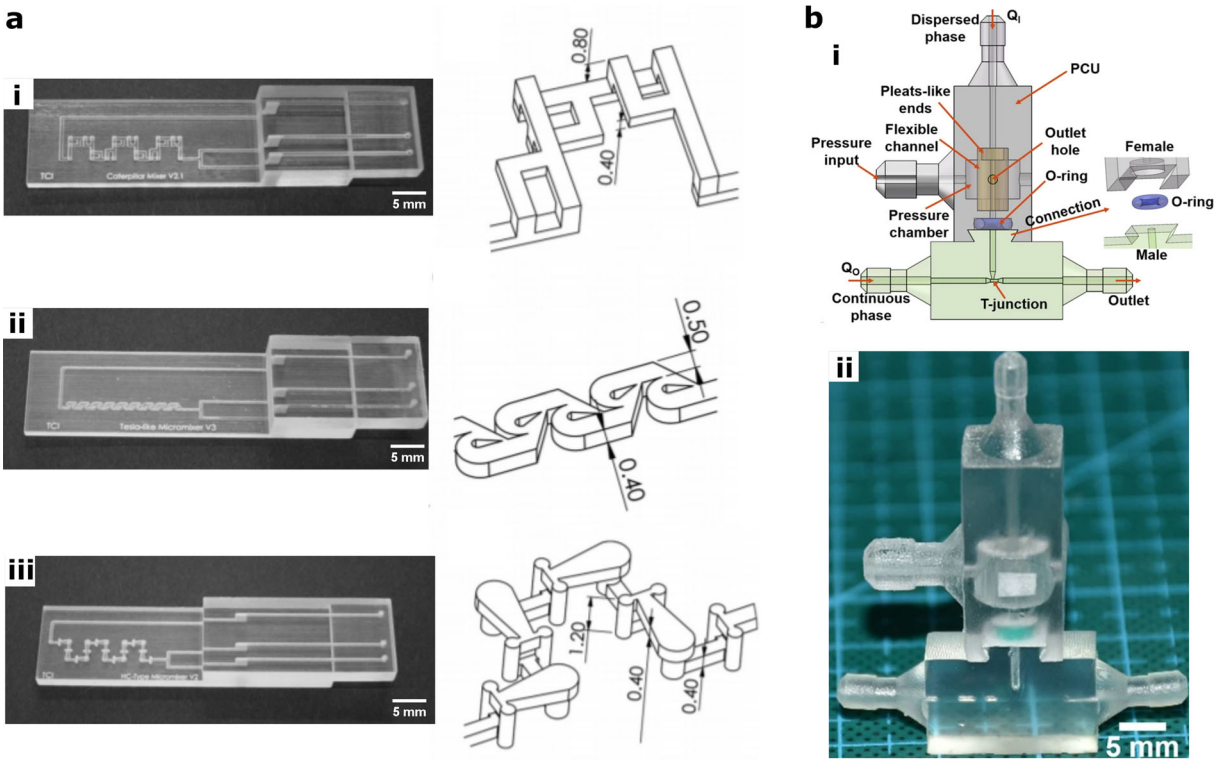

Fig. 10 Microfluidic devices fabricated with inkjet–direct printing approach (**a**) various mixing devices fabricated with the multijet printer: (i) 3D printed caterpillar mixer (left), dimensions of the channels (right), (ii) 3D printed Tesla mixer (left), dimensions of the channels (right), (iii) 3D printed HC mixer (left), dimensions of the channels (right). (**b**) Multimaterial droplet generator fabricated with the polyjet printer: (i) schematic of the device, (ii) 3D printed droplet generator. Panel (**a**) is reproduced from [94] with permission of John Wiley and Sons. A scale bar has been added based on channel size reported. Panel (**b**) is reproduced from [97] under the Creative Commons Attribution 4.0 International Public License (https://creativecommons.org/licenses/by/4.0/)

control unit to control droplet generation. Moreover, such multi-material 3D printing can also be used to integrate microvalves fabricated from a flexible material and other structures from a rigid material in a microfluidic device [98].

Microfluidic devices fabricated by inkjet 3D printing: mold-based approach

Both sacrificial and non-sacrificial molds can be fabricated with the inkjet printing method.

Kamei et al. used 3D printed microchannel molds to fabricate PDMS devices for culturing human embryonic stem cells encapsulated in the hydrogels under a gradient of human basic fibroblast growth factor [99].

Glick et al. introduced a multi-sided molding technique in which both the upper and lower molds were used to transfer features to PDMS [100]. This particular technique enabled the fabrication of thin membrane valves, devices with fluid flow in 3-dimensions, and multilayer devices. Moreover, they recommended the silanization process to inhibit PDMS adhesion to the mold surface.

Brossard et al. used hexanediol ink material and a custom-made inkjet printer to fabricate sacrificial molds for microfluidic devices [101]. Hexanediol ink was printed on a substrate kept at 5 °C, allowing the ink to freeze. Finally, the molds were cast with PDMS and subsequently evaporated at an elevated temperature. The minimum channel width of 50 μm was achievable with this method.

Hwang et al. 3D printed molds for fabricating non-planar PDMS microchannels [102]. They reported higher surface roughness on the 3D printed masters printed with polyjet compared to conventional SU-8 masters, which is a limitation associated with the polyjet technology. Moreover, inkjet printing has also been used for producing sacrificial wax molds for PDMS replica molding [103].

Hybrid approach

Fabrication of hybrid devices has been demonstrated majorly with FDM and SLA 3D printing technologies. This section discusses a few bonding techniques used to form hybrid devices and how a hybrid approach can overcome some of the limitations of a direct printing approach.

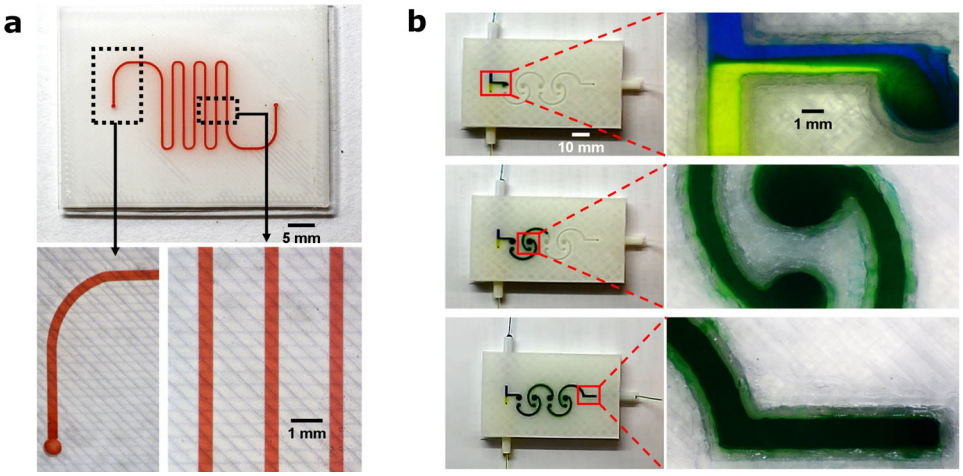

Fig. 11 PLA/PMMA hybrid microfluidic devices (**a**) serpentine microchannel. (**b**) mixing at different locations in the hybrid 3D printed mixing device. Panels (**a**) and (**b**) are reprinted from [111] Copyright 2018, with permission from Elsevier. A scale bar has been added in (**a**) and (**b**) based on overall dimensions and feature size reported

FDM hybrid devices

Microchannels printed with FDM direct printing approach are often found opaque under an optical microscope owing to the rough layers printed on the channels. Therefore, an alternative approach can be used wherein the microfluidic device can be printed with open microchannels (without any layers on top of them), and transparent materials such as PMMA and PDMS can be bonded on the top for better visibility of 3D printed channels. Integration with PDMS improves the visibility of the channels and allows better control of the gaseous environment inside gas-impermeable polymers. Here, we have elaborated on different methods to bond 3D printable FDM polymers and transparent materials to fabricate hybrid microfluidic devices.

Thermoplastic polymers such as polycarbonate (PC), cyclic olefin copolymer (COC), polymethylmethacrylate (PMMA), polystyrene (PS), and polyethylene terephthalate (PET) can be irreversibly bonded with PDMS using (3-aminopropyl)triethoxysilane (APTES) [60, 104–107]. Tang et al. used an amine-epoxy bond formation strategy to bond polymers with PDMS [108]. Moreover, Mehta et al. used a chemical-free bonding method wherein plasma treatment with a combination of oxygen and argon gases (2:1) was used to bond polymers with PDMS [40].

Moreover, bonding between different thermoplastic polymers can also be achieved by activating the surfaces of polymers with UV/ozone treatment followed by heating at glass transition temperature under pressure [109]. This approach can be applied for bonding 3D printed microfluidic devices with PMMA.

Ethanol-based solvent bonding technique can be used for bonding PMMA with 3D printed polymers. In this method, PMMA and 3D printed polymers (ABS and PLA) were coated with ethanol and irradiated with UV light [110, 111]. UV light irradiation dissolved PMMA and generated acrylate monomers, which eventually bonded the two polymers. With this method, authors have fabricated a hybrid serpentine channel (Fig. 11a), a mixing device (Fig. 11b), and a double emulsion generator.

Owing to the similar chemical structure, PLA can be readily bonded to PMMA by direct 3D printing of PLA on the PMMA substrate. Such PLA-PMMA hybrid devices have been used to determine total proteins, nitrite, nitric oxide, and producing nano-particles [36, 112].

SLA hybrid devices

Microfluidic devices printed with SLA direct printing approach suffer from low optical transparency, blockage of the channels due to trapped uncured resin, and low gas permeability. The hybrid approach makes SLA microchannels' cleaning procedure relatively faster and more reliable as the channels are accessible from the top and are not embedded inside the device.

Recently, Kecili et al. demonstrated the bonding of SLA printed devices (Formlabs form 2) with glass slide using PDMS or resin interlayer [113]. Moreover, SLA printed open-faced microchannels can also be bonded with PDMS using APTES or silicon spray [114]. These hybrid SLA devices were used for gradient and droplet generation.

Cheon et al. tested five different bonding methods, namely double-sided tape, PDMS/tape composite, UV glue, (3-aminopropyl) triethoxysilane (APTES), and sputter-coated SiO_2 for bonding 3D printed devices with PDMS [37]. They found that the sputter coating produced the highest burst pressure compared to other techniques.

Brennan et al. used an intermediate layer based bonding method to bond PDMS membrane with watershed resin parts to allow oxygen control for the cell culture [38]. In addition to the intermediate layer based bonding method, watershed resin parts can also be bonded with PDMS by activating PDMS with plasma treatment and heating the hybrid

Table 1 Applications of four fundamental approaches

3D printing technology	Approach used	Material used	Applications	References
FDM	Direct printing approach	TPU	Flexible and biocompatible microfluidic devices	[28]
		PLA, PETg	Transparent microfluidic devices such as mixing and droplet formation devices, core–shell metallic nanoparticles generator, devices with embedded glass coverslips, porous membranes, electrodes, and wires	[45, 48, 49, 51]
		PP	Reactionware devices for chemical synthesis and nanoparticle synthesis	[46, 47]
		ABS, Lay-felt composite filament	Multi-material devices with integrated membrane for colorimetric detection of nitrate in the soil	[50]
	Mold-based approach	Sacrificial molds form ABS	Spiral channels, channels with varying diameters, Hilbert cube, devices integrated with electronic components, channels with unconventional shapes such as triangular and semielliptical	[54, 55]
		Sacrificial molds from PVA	Droplet forming devices, devices for dynamic cell culture, chaotic mixing devices	[56]
		Sacrificial molds from PVA and HIPS	Microfluidic devices with over-hanging and helical features	[57]
		Non-sacrificial molds from ABS	Droplet generators, gradient generators, and devices with 3D crossover features	[58]
	Modular approach	PLA	Droplet forming device, dental pulp stem cells encapsulation device, gradient generator, devices for a dynamic culture of cells and degradation of bone scaffold	[59–61]
	Hybrid approach	PLA-PMMA and PLA-ABS	Emulsion generator device, mixing device	[110, 111]
		PLA-PMMA	Devices for determination of total proteins, nitrite, nitric oxide and for producing nanoparticles	[36, 112]
Non-filament-based extrusion	Direct Printing approach	Silicone sealant	Serpentine mixer, droplet generator, Y channel, air–liquid interface cell culture device, devices integrated with electronic components	[62]

Table 1 continued

3D printing technology	Approach used	Material used	Applications	References
		PCL	Liver-on-a-chip, nervous system-on-a-chip	[39, 63]
	Mold-based approach	Wax	Interconnected 3D mixing units, self-healing microvascular network	[64, 65]
		Sugar	Spiral, serpentine, 3D microchannels, cell culture device, devices with the microvascular network, combinatorial mixer generator	[66–68]
		Pluronic F127	Devices with three-dimensional microvascular networks, vascularized heterogeneous tissue constructs	[69, 70]
		Agarose	Tissue with vascularized networks	[71]
SLA	Direct printing approach	Proprietary colorless resin	3D mixer, 3D gradient generator, droplet extractor, ITP separation device, and tapwater nitrate analysis device	[27]
		PEG-DA	Serpentine channel, chaotic mixers, microvalves, cell culture devices, high-resolution capillary channels	[73–76, 79]
		PDMS	Biocompatible microfluidic devices with 500 μm channels	[77]
		WaterShed XC 11122 (DSM)	Devices with integrated microvalves, osteochondral bioreactor	[78, 83]
		Transparent resin (Formlabs)	Microfluidic devices for 3D cell culture inside hydrogel	[84]
		Accura 60 (3D systems)	Devices for spheroid culture	[85]
		E-shell 300 (EnvisionTEC)	Osteochondral tissue culture bioreactor	[8]
		PIC100, HTM-140 (EnvisionTEC)	Droplet generators and Nanoliposome generators	[80, 81]
		Bisphenol A ethoxylate diacrylate (BEDA)	Microfluidic device for early cancer detection	[82]
		Pro3dure GR-10	Tumor-on-a-chip	[115]
	Mold-based approach	Proprietary resin	3D chaotic mixer, devices with overhanging features, devices integrated with microvalves	[19]
		Black resin (Formlabs)	Device for studying the interaction between leukocytes and TNFα-activated endothelial cells	[88]
		Clear resin (Formlabs)	Multi-depth droplet generator devices	[89]

Table 1 continued

3D printing technology	Approach used	Material used	Applications	References
		BV-007 (Miicraft)	Lung-on-a-chip	[116]
		Grey resin (Formlabs)	Spheroid forming device with gradient of diameter	[117]
		Accura extreme (3D systems)	Spheroid forming device with uniform diameter	[118]
	Modular approach	WaterShed XC 11122 (DSM)	Droplet generators, mixing devices, reaction chambers	[29, 34]
		R5 Gray, ABS 3SP Flex Gray (EnvisionTEC)	Lego® like PDMS blocks stacked to form multilayer microfluidic devices	[35]
	Hybrid approach	WaterShed XC 11122-PDMS	Cell culture device with oxygen control, device for stimulation of cells with ATP solutions	[38, 78]
		Clear resin (Formlabs) -PDMS	Gradient and droplet generators	[114]
Inkjet	Direct printing approach	VisiJet M2R-CL (3D Systems)	Caterpillar mixer, Tesla mixer, HC mixer	[94]
		Objet VeroWhitePlus (Stratasys)	Device for studying drug transport and the effect of drugs on cells	[95]
		Veroclear and TangoPlus FLX930 (Stratasys)	Emulsion generator device	[97]
		VeroWhitePlus and TangoPlus FLX930 (Stratasys)	Devices with integrated microvalves	[98]
		Verowhiteplus RGD835 (Stratasys)	Micro and nanoparticle collection and analysis	[96]
	Mold-based approach	AR-M2 (Keyence)	Hydrogel encapsulated cell culture devices	[99]
		VisiJet EX200 (3D systems)	Multi-sided molds for fabricating microfluidic devices	[100]
		Hexanediol	Serpentine channels, combinatorial mixer, overhanging channels, integration with electrodes	[101]
		VeroWhitePlus (Stratasys)	3D microfluidic channels	[102]

device above the glass transition temperature of watershed resin [78].

As discussed above, there are few published protocols already available for fabricating SLA hybrid devices. However, proprietary resin composition necessitates further experiments to find a suitable bonding protocol for each of them.

Table 1 summarizes the applications of four fundamental approaches for fabricating microfluidic devices.

Challenges with 3D printing of microfluidic devices

3D printing is still considered a secondary manufacturing technique for microfluidic devices as there are few challenges associated with the same that need to be addressed. One of the challenges is a printing resolution, which is still inferior to the conventional photolithography technique. Moreover, low optical transparency, low gas permeability, and cytotoxicity of the 3D printing materials are three of the major roadblocks which hinder the widespread use of 3D printing. In this section, we have highlighted such limitations and discussed the recent research progress in the 3D printing materials and

technologies, which improved the overall performance of 3D printed microfluidic devices.

Printing resolution: from millifluidic to microfluidic range

Currently, the majority of the commercial 3D printers are capable of printing channels within millifluidic (> 1 mm) and sub-millifluidic range (> 500 μm) but not in the microfluidic range (< 100 μm) (Table 2) [76]. Although many SLA manufacturers claim an XY resolution of less than 100 μm, the printable microchannels are often higher than 100 μm [26, 27, 119].

The smallest channel width is one of the parameters to evaluate the 3D printer's XY resolution for fabricating microfluidic devices. XY resolution of the FDM 3D printer is limited by nozzle diameter and the smallest movement of X and Y stepper motors. Nelson et al. reported the smallest channel size (40 μm) for FDM 3D printing (Table 2) [28]. They used a nozzle of 250 μm diameter on Prusa i3 MK3 3D printer (Prusa Research, Prague, Czech Republic). Along with a smaller nozzle size, the distance of a nozzle from the printing bed and printing temperature also plays a significant role in determining the minimum channel size. Longer printing times and frequent nozzle clogging are some of the limitations associated with smaller nozzle diameters.

Table 2 shows most of the minimum channel sizes reported for direct, modular, and hybrid approaches (in the case of extrusion-based 3D printing) are comparatively higher than the mold-based approach. This is because, in a mold-based approach, the channels' width can be directly controlled by nozzle diameter, pneumatic pressure (extrusion flow), and printing speed (Eq. 1 in microfluidic devices fabricated by non-filament method: mold-based approach section). For example, He et al. reported a 40 μm channel width by controlling printing speed and using a nozzle diameter of 300 μm [66]. However, printing a 40 μm channel void is challenging with 300 μm nozzle size in direct, hybrid, and modular-based approaches. This is because of the limitations of nozzle diameter, the smallest movement of stepper motors, the distance of nozzle from the printing bed, and printing temperature. Besides, microchannels with 18 μm diameter could be achieved using a nozzle of 30 μm diameter and controlling the pressure of extrusion in a mold-based approach [69].

In conventional stereolithography, the XY resolution is controlled by laser spot size, overall optical system, and curing mechanism. But in DLP-SLA printers, the XY resolution is mainly controlled by minimum pixel size. Earlier, it was challenging to fabricate channels less than 100 μm with stereolithography. However, with the recent improvements in the absorbance properties of PEG-DA resin, superior XY resolution of the custom DLP apparatus (7.6 μm), and 385 nm UV curing mechanism, researchers have successfully 3D

Table 2 Four fundamental approaches and the smallest channel width reported

3D printing technology	Approach used	The smallest channel width reported (in μm)	References
FDM	Direct printing approach	40	[28]
		400	[45]
		1000	[48]
		800	[47]
		600	[49]
		260	[51]
		800	[47]
	Mold-based approach	200	[54]
		100	[55]
		232	[56]
	Modular approach	500	[59]
		400	[60]
		118	[61]
	Hybrid approach	170	[36]
		500	[111]
		389	[112]
Non-filament-based extrusion	Direct printing approach	635	[62]
		1500	[39]
	Mold-based approach	200	[65]
		40	[66]
		150	[67]
		18	[69]
		100	[70]
		150	[71]
SLA	Direct printing approach	250	[27]
		27	[74, 75]
		20	[76]
		500	[77]
		350	[79]
		600	[83]
		500	[84]
		354	[115]
	Mold-based approach	300	[19]
		208	[88]
		150	[89]
	Modular approach	500	[29]
		635	[34]
		500	[35]
	Hybrid approach	228	[114]
Inkjet	Direct printing approach	130	[94]
		239	[97]
		400	[98]
	Mold-based approach	50	[101]
		500	[102]

printed the smallest microchannel with a cross section of 18×20 μm (Table 2) [76]. Similarly, Kim et al. reported microchannels with a width of 27 μm using a commercial high-resolution DLP printer Asiga Pico2 HD (Asiga, Sydney, Australia) (XY resolution—27 μm) [75]. Moreover, low resin absorbance is one of the major parameters affecting the Z resolution of SLA and DLP printers. Because of the low absorbance of transparent resins in the visible light spectrum, the commercial printers with a 405 nm light source often cure the microchannel voids, blocking the whole microchannel, thereby providing a poor Z resolution [73]. To improve the Z resolution, in-house formulated PEG-DA-based resins with optimized absorbance properties, and a 385 nm UV curing source has been used [74, 76, 120, 121].

In inkjet printing, droplet size is one of the parameters that controls minimum channel size. Brossard et al. recently reported the smallest channel size of 50 μm channels with hexanediol ink and a custom-made inkjet system (Table 2) [101]. The custom-made inkjet printer could generate droplets of 50 μm size with droplet spacing of 40 μm.

Optical transparency

FDM uses transparent materials such as PETg to fabricate microfluidic devices. While printing with such transparent filaments, air bubbles often get trapped inside the layers, which scatter the light and make the devices opaque. Many research groups have tried to optimize a few FDM parameters to improve the overall optical transparency of the microfluidic devices. These parameters include layer height, printing speed, printing temperature, cooling rate, nozzle distance from the build platform, and extrusion flow. Lowering printing speed, layer height, and nozzle distance from the bed have been found to increase the optical transparency of microfluidic devices [28, 45, 59, 122]. Moreover, integration with transparent glass coverslips and PMMA sheets have also been found to improve the visibility of the microchannels printed with FDM [36, 48, 49, 112].

Moreover, 3D printers often use rough build surfaces for improving the adhesion of the first layer. Such rough build surfaces produce high surface roughness on the base layer of microfluidic devices, making them opaque. Mechanical sanding and polishing have been effective in reducing the base layer roughness and enhancing the visibility of the microchannels [84, 115]. Sometimes, the optical transparency of SLA microchannels can be compromised due to the poor absorbance of the resin and laser over-curing, which can be mitigated by coating microchannels with various mineral oils to match the refractive indices of the resins [26, 84].

Biocompatibility and post-processing

The biocompatibility of the resins is a critical parameter for biological applications of 3D printed microfluidic devices. There are many biocompatible resins available from various manufacturers such as E-shell 300 series (EnvisionTEC, Germany), WaterShed XC 11,122 (DSM, Netherlands), MED625FLX (Stratasys, USA), Dental SG (Formlabs, USA), and Pro3dure GR-10 (Pro3dure Medical GmbH, Germany). The proprietary formulation of these resins often necessitates thorough biocompatibility evaluation for the intended biological application [115]. One of the research studies found growth inhibition of freshwater microalgae caused by SLA and inkjet resins, including biocompatible WaterShed XC and VisiJet crystal resin (3D systems, USA) [123]. On the contrary, FDM materials such as PLA and ABS did not produce any toxic effects in the same study. In another study, C_2C_{12} cells remained viable for five days and showed morphological alignment on 3D printed FDM polymers [124].

Because of the questionable biocompatibility of the commercial resins, researchers have started moving toward in-house formulated biocompatible resins for 3D printing of microfluidic devices [73, 74, 121].

Post-processing plays a significant role in preventing or delaying the toxic effects of the resins. For example, PEG-DA resin is biocompatible only after extensive post-processing steps, including washing uncured resin and UV post-curing [73, 74]. Without the post-processing steps, toxic monomers and photoinitiators can leach over time, causing cytotoxicity. Moreover, PDMS devices produced by 3D printed SLA molds have also shown toxic leachates possibly transferred from the resin used for fabricating the molds [125]. The coating of microchannels with PDMS, cell culture media, or polystyrene has been effective in slowing down the leaching of such toxic substances from the resin [74, 125–127].

One of the commercial biocompatible resins, Pro3dure GR-10, can be a promising candidate for fabricating microfluidic devices for biological applications. In one study, it did not show any cytotoxic effects up to 14 days and genotoxic effect for 30 days [128]. Microfluidic devices fabricated from Pro3dure GR-10 have also been used to culture biopsy tumor tissues for at least three days in a microfluidic device [115].

There is a need for introducing commercial novel biocompatible materials with relevant cytotoxicity data to encourage the use of 3D printed microfluidics in the biological field.

Surface roughness and bonding

Roughness comes inherently with 3D printing due to the layer-by-layer fabrication approach. The average surface roughness of the FDM devices was found to be the high-

est (R_a = 10.97 μm), compared to inkjet (R_a = 0.99 μm) and SLA-based techniques (R_a = 0.35 μm) [129].

Higher surface roughness is one of the major drawbacks of FDM. There are few post-processing methods available, such as polishing, painting, vapor smoothing, solvent dipping, and epoxy coating, to reduce the overall surface roughness of FDM components [130]. Tsuda et al. demonstrated dichloromethane vapor treatment to smooth 3D printed PET and PLA surfaces [60]. Moreover, Lalehpour et al. carried out an extensive analysis of the acetone vapor smoothing process for ABS parts [131]. They found three cycles with 15 s treatment of acetone vapor produced the best surface finish. Although there are few reports on post-processing methods for FDM components, systematic research studies and novel ways to reduce roughness are still lacking.

Roughness on inkjet soft lithography molds often prevents the bonding of replica molded microchannels with glass coverslips or PDMS blocks. Glick et al. suggested to spin coat liquid PDMS on the replica molded surface [100]. The liquid PDMS works as filler for small crevices present on the surface and a bonding agent for bonding replica molded microfluidic devices with glass coverslips or PDMS blocks. Moreover, for making soft lithography molds with polyjet printing (Stratasys), the glossy finish option has been recommended over the matte finish option [102]. In multijet printers (3D systems), omniphobic lubricant infused coating has been beneficial to mitigate surface roughness on the soft lithography molds [132].

In stereolithography molds, the printing orientation affects the surface roughness significantly. For example, molds printed parallel to the build surface were smoother than molds printed at an angle [88].

Wettability

Wettability of PDMS can be controlled by plasma, corona, or UV/ozone surface treatment methods [133, 134]. PDMS channels can be made hydrophilic by such surface treatment methods to introduce the reagents in the microchannels using capillary effect without any need for external pumping. The capillary filling is one of the desirable properties for microfluidic device operations. FDM polymers can be made hydrophilic using UV/ozone and plasma surface treatment methods [17, 133]. Few reports suggested the possibility to activate surfaces of SLA devices using oxygen plasma and corona discharge treatment methods [37, 135]. However, further investigations are required to characterize the effect of such treatment methods on microchannels fabricated by stereolithography and inkjet 3D printing.

Autofluorescence and optical microscopy

The autofluorescence of polymers can be a barrier for fluorescence microscopy. Salentijn et al. investigated the autofluorescence of various FDM materials and found all the polymers exhibited autofluorescence to some extent [52]. Moreover, they found the FDM polymers exhibited the least autofluorescence at red wavelengths. Stereolithography resins such as PEG-DA-based resin and WaterShed XC resin showed a low level of autofluorescence [26, 74]. Moreover, Pro3ure-GR 10 resin did not show any autofluorescence [115]. Autofluorescence can lead to an erroneous analysis of fluorescence images. Therefore, it is necessary to develop novel 3D printing materials with low or negligible autofluorescence.

Sterilization

Sterilization with short-wavelength UV light has been used widely for PDMS microfluidic devices. However, FDM polymers are not as transparent as PDMS to germicidal UV-C light. Moreover, many of the FDM materials are non-compatible with autoclave sterilization as the glass transition temperatures of such polymers lie below 121 °C. Alternative sterilization techniques for FDM parts include ethylene oxide gas, hydrogen peroxide gas plasma, immersion in ethanol, and gamma irradiation [136]. Some of the FDM materials which are compatible with autoclave sterilization are Nylon PA 12 (Forecast 3D, USA), PC-ISO (Stratasys, USA), ULTEM-9085 (Stratasys, USA), PPSU (Stratasys, USA), and Nylon 680 (Taulman 3D, USA) [136, 137].

SLA and inkjet materials also exhibit lower heat deformation temperatures, thereby restricting the use of autoclave sterilization method. However, a few resins are available that can be autoclaved, such as Pro3ure GR-10 [138] and Dental SG [139]. The general unavailability of 3D printing materials compatible with autoclave often discourages researchers from using 3D printing to fabricate microfluidic devices. Therefore, novel materials compatible with autoclave sterilization are needed to be developed.

Gas permeability

3D printed polymeric microfluidic devices often create a hypoxic environment inside the channels within a few hours because of their gas impermeability [40, 140]. Therefore, it is challenging to maintain a proper gaseous environment for cell growth inside such 3D printed microchannels. Using a hybrid approach with integration with gas permeable PDMS can be beneficial for long-term cell growth inside 3D printed microchannels. Moreover, dynamic perfusion with a syringe pump can also be effective in replenishing depleted oxygen concentration inside such polymer microchannels [140].

However, long-term dynamic perfusion may lead to air bubble formation in the channels, causing cell death [141]. We believe the development of novel gas permeable 3D printing materials will be one of the major research areas in this field.

Table 3 summarizes the limitations associated with 3D printing of microfluidic devices with possible solutions to overcome them.

The state of 3D printed 'organs-on-chips' and 'tumor-on-chips': present and future

3D printed organs-on-chips: the current state

Complex tissues with multiple cell types can be effectively mimicked using 'organs-on-chips' [3–6]. Many research groups have demonstrated such models, which can bring down the failure rate of the drugs in the clinical phase and can be a promising alternative to in vivo animal drug testing in the future. In this section, we have discussed some of the remarkable 3D printed organ-on-a-chip models to highlight the potential of existing 3D printing technology.

Organs-on-chips using extrusion-based 3D printing

Current in vivo models often fail to predict the toxic effects of novel drugs on humans. Hence, there is a need to develop 3-dimensional, functional, and dynamic liver-on-a-chip models. Bhise et al. 3D printed hepatic spheroid-laden hydrogel constructs inside the microfluidic device and demonstrated its functionality for 30 days [142]. Moreover, acetaminophen's drug toxicity predicted by the developed platform was found similar to in vivo data. Lee et al. 3D printed a liver-on-chip platform using PCL and cell encapsulated hydrogels [39]. PCL was printed to make microfluidic channel structure, and cell encapsulated hydrogels were printed to spatially pattern Human hepatocellular carcinoma cell line (HepG2) and human umbilical vein endothelial cells (HUVEC) in various orientations.

Kolesky et al. used a sacrificial mold-based approach to fabricate thick vascularized tissues containing endothelial cells, fibroblasts, and stem cells [143]. They had cultured and differentiated the stem cells by delivering growth factors through the printed vascular network. This particular approach is suitable for developing physiologically relevant vascular liver models where the cell-laden ink can be used to print hepatocytes, and the supporting casting matrix can contain the immune cells.

Gu et al. used an extrusion-based technique to develop neural tissues from human neural stem cells laden hydrogels [144]. They used novel polysaccharide-based bioink, which provided stable and rapid cross-linking. This strategy can be implemented on microfluidic devices to develop neural disease models. Johnson et al. fabricated neuron-on-a-chip platform, consisting of 3D printed microchannels for axonal alignment and compartmented tri-chamber for cell isolation and co-culture of neurons, glia, and epithelial cells [63].

Organs-on-chips using stereolithography

Ma et al. used stereolithography to mimic the hexagonal architecture of the liver lobule [145]. This process uses two different masks fed sequentially for patterning hepatic cells and supporting cells (endothelial cells and stem cells).

Lin et al. 3D printed bioreactor to culture osteochondral tissue and model osteoarthritis [8]. The bioreactor inserts isolated chondral and osseous regions by an O-ring and supplied chondrogenic and osteogenic differentiation media in upper and lower chambers, respectively. Upon treatment with pro-inflammatory cytokine (IL-1β), osteoarthritis like response was observed in both the tissues.

Stereolithographic molds are being used widely for fabricating organs-on-chips. Shrestha et al. used SLA molds to fabricate lung-on-a-chip device [116]. The design involved an upper PDMS layer containing a chamber for culturing Calu-3 cells and the lower PDMS layer containing a microchannel to perfuse the media. Both layers were bonded with a porous polycarbonate membrane aligned in the middle. The secretion of inflammatory cytokines upon treatment with cigarette smoke extract validated the in vitro model.

Donald Ingber's research group has extensively used SLA molds for fabricating organ-on-a-chip such as liver-on-a-chip [146], blood–brain barrier chip [147], bone marrow-on-a-chip [148], and lung airway-on-a-chip [149]. The design usually involves a two-layered PDMS device consisting of two microchannels separated by PET or PDMS membrane. The upper channel is used for culturing parenchymal cells, and the lower channel acts as a stroma with endothelial cells, fibroblasts, and immune cells.

3D printed organs-on-chips: the future

We think multi-material 3D printers with the capability to spatially pattern various cells, dynamically mix two or more materials, and print with hard and soft materials will open the doors for the rapid development of physiologically relevant organs-on-chips.

Many researchers have demonstrated extrusion-based mixing heads, which can mix two or more materials in varying ratios to fabricate functionally graded materials with a smooth variation of physical and chemical properties [150–152]. Such mixing heads will be useful in producing biological composites and developing organs-on-chips with gradients of properties found in natural interface tissues [153]. For example, a multi-material printer with the capability to mix hard and soft materials can be used to fabricate the

Table 3 Limitations associated with 3D printing of microfluidic devices with reported solutions

Approach	Limitations	Reported solutions
Direct printing approach	**FDM**	
	Sagging of polymers in the bridging layer	Use of non-rectangular cross sections such as elliptical, circular, and triangular [28]
	Low optical transparency	Integration of glass cover slips and PMMA [36, 48, 49, 112], optimization of various FDM parameters [28, 45, 59, 122]
	Leakage from the channels	Use of 100% Infill density
	Low XY resolution	Use of fine nozzle diameter
	High surface roughness	Use of low layer heights, mechanical polishing, vapor smoothing [60, 130, 131]
	Hydrophobicity	Plasma and UV/ozone treatments [17, 133]
	SLA	
	Low optical transparency (laser over curing) and low Z resolution	Optimization of absorbance properties of the transparent resins and use of 385 nm UV curing source [73, 74], Coating of microchannels with various mineral oils [26, 84], Use of hybrid approach (Integration with PDMS)
	Poor biocompatibility	Use of proper post-processing steps to get rid of uncured resin monomers [73, 74] Coating of microchannels with PDMS, wax, cell culture media, or Polystyrene [74, 125–127]
	Hydrophobicity	Plasma and corona discharge treatments [37, 135]
	Trapped uncured resin	Use of a hybrid approach to remove resin from the channels easily
	High surface roughness	Mechanical polishing [84, 115]
	Some common problems:	
	Non-compatibility with autoclave sterilization	Use of other sterilization methods such as ethylene oxide gas, Hydrogen peroxide gas plasma, immersion in ethanol, and gamma irradiation [136]
	Low gas permeability	Integration with PDMS [38, 78], dynamic perfusion [140]
Mold-based approach	**FDM**	
	High surface roughness	Integration with glass coverslips, vapor smoothing, and polishing [48, 58]
	SLA	
	Uncured PDMS and PDMS adherence to the mold surface	Post-processing steps including heating and silanization [19], use of methacrylate-based resins [87]
	High surface roughness	Printing mold parallel to the build surface [88]
	Inkjet	
	PDMS adherence to the mold surface	Silanization [100]
	High surface roughness	Spin coating of PDMS on the mold [100], Use of glossy finish option in polyjet printers [102], Use of omniphobic lubricant infused coating [132]
Modular approach	Fluid leakage	Use of O-rings between two fluidic modules [59], reduction of overall roughness [35, 60], use of capillary driven open microchannel systems [61]
Hybrid approach	Failed bonding	Use of various methods to reduce the overall roughness, as suggested above

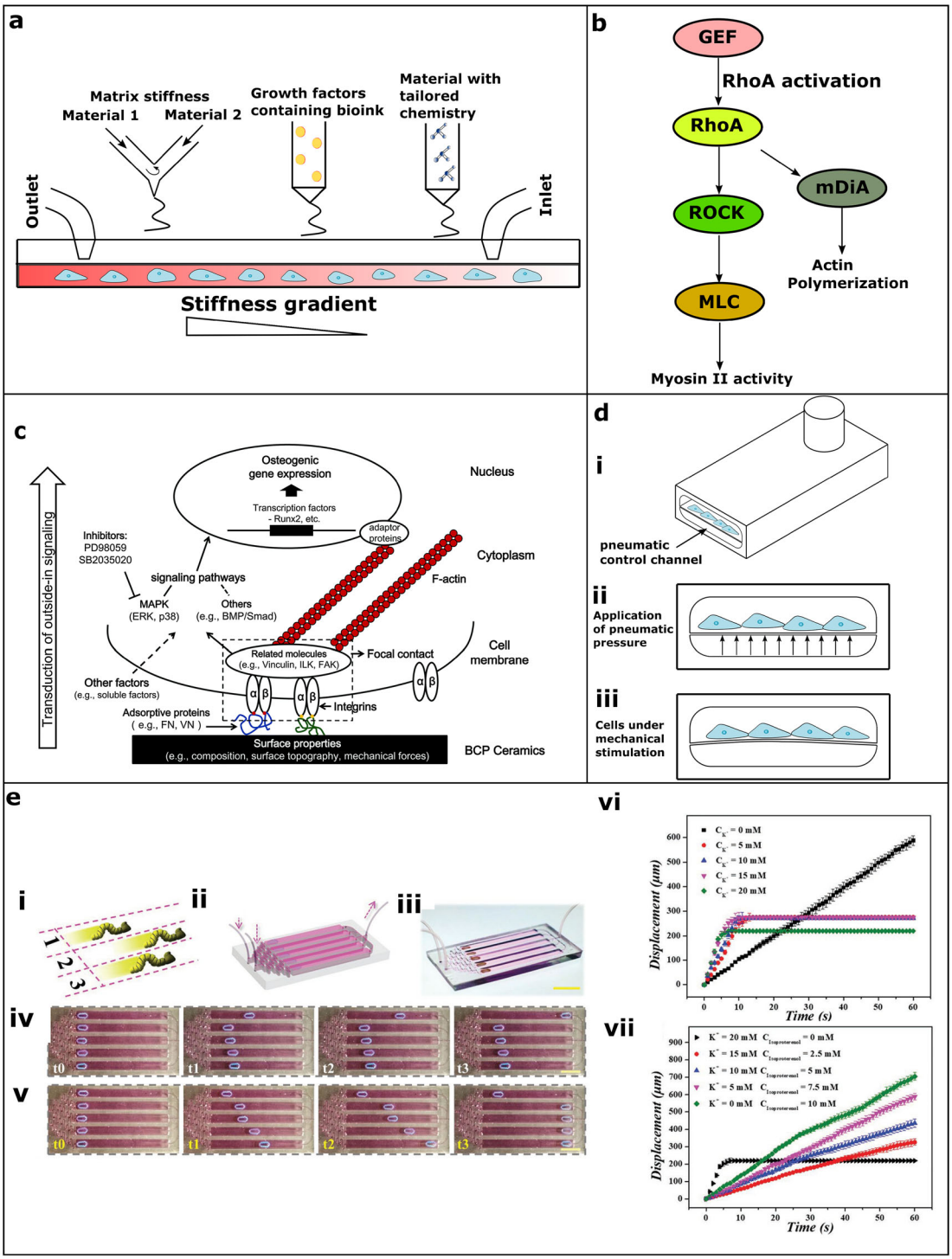

Fig. 12 3D printed organs-on-chips: The future (**a**) illustration of a multi-material printer with dynamic mixing head for modulating the stiffness of matrix, growth factor printing head, and head for surface functionalization for guided stem cell differentiation. (**b**) RhoA/ROCK molecular pathway (**c**) MAPK molecular pathway (**d**) (i) cross section of a microchannel having a thin membrane-like layer isolating cell culture chamber and pneumatic control chamber printed with stereolithography, (ii) front view of the printed device, (iii) pneumatic pressure deforming the 3D printed membrane structure to apply mechanical stimulation to the cultured cells. (**e**) Heart-on-a-chip integrated with a soft robotic system. (i) Schematic of caterpillar racing track based on the chemical stimulus, (ii) schematic of the PDMS microfluidic system with soft robots, (iii) optical image of a microfluidic system with soft robots, (iv,vi) under the chemical stimulus of potassium-ion solution. (v,vii) under the chemical stimulus of potassium-ion and isoproterenol solution. The scale bars for (**e**): 2 cm in (iii) and 1 cm in (iv) and (v). Panel (**b**) is adapted with permission from [163]. Copyright 2012 American Chemical Society. Panel (**c**) is reproduced from Ref. [171] with permission from The Royal Society of Chemistry. Panel (**e**) is reproduced from [178] with permission of John Wiley and Sons

cartilage-on-a-chip platform with a stiffness gradient found in the cartilage tissue (Fig. 12a) [154].

Moreover, the ability to integrate hard and soft materials in one microfluidic device can be utilized in developing 3D printed blood vessels-on-a-chip, in which blood vessels can be made with soft materials, and other microfluidic physical structures can be made with hard materials.

Moreover, with multi-head bioprinters, now it is possible to spatially pattern different cell-laden hydrogels mimicking the heterogeneous tissues [155, 156]. As shown by Lee et al., multi-material based approaches enable faster fabrication of more realistic organs-on-chips in one step [39].

Multi-material 3D printing will also support in vitro guided differentiation of stem cells on a microfluidic chip by incorporating various physical signals including matrix stiffness, topography, porosity, and chemical signals including material chemistry, cell adhesive ligands, and various growth factors in a cell-laden biomaterial [157–159] (Fig. 12a). Such biological cues can be incorporated in the form of a gradient in a microfluidic device for multiphase tissue development from stem cells like osteochondral tissue [8, 160].

Biomaterials with a range of stiffness values influence stem cell differentiation into a specific lineage [158, 161]. Cells can sense the matrix stiffness by applying traction force on the matrix, transmitted through the assembly of focal adhesion proteins and integrins [158]. Few molecular pathways behind sensing and responding to such mechanical signals have been identified, including small GTPases (guanosine triphosphatase), tyrosine kinases, and ion channels. Activation of Rho GTPases, especially RhoA, is one of the most studied mechanotransduction pathways (Fig. 12b). RhoA is responsible for regulating the activity of myosin II in stress fibers and intracellular forces generated in cells [162]. After alteration of RhoA from an inactive GDP-bound state to an active GTP-bound state by regulatory guanine nucleotide exchange factors (GEFs), RhoA phosphorylates Rho-associated protein kinase (ROCK) [158]. ROCK phosphorylation leads to the activation of myosin light chain (MLC). MLC activation leads to the assembly of myosin II into bipolar filaments, which is responsible for cell contractility [158, 163]. Moreover, RhoA also promotes actin polymerization by binding to mDiA [164].

RhoA/ROCK pathway controls stem cell lineage commitment in association with shape and cytoskeleton tension [165, 166]. The study by McBeath et al. found that regulating RhoA activity led stem cell differentiation to osteoblasts (by activating RhoA) or adipocytes (by inactivating RhoA) without any differentiation factors [166]. However, RhoA-mediated stem cell differentiation required spread cell shape for osteogenesis and round cell shape for adipogenesis. Interestingly, they also found that activation of RhoA effector ROCK can make stem cells differentiate to osteoblasts independent of cell shape, which implies that ROCK-induced tension generating system is required for cell-shape mediated stem cell differentiation to osteoblasts.

Apart from physical cues, biomaterial surface chemistry plays a major role in the guided differentiation of cells. Keselowsky et al. demonstrated surface chemistry-based osteoblast differentiation and mineral deposition [167]. They found that -NH_2 and -OH groups upregulated osteoblast-related gene expression compared to -COOH and -CH_3 functional groups. Furthermore, surface chemistry-related osteoblast differentiation was due to specific integrin receptor binding to the absorbed fibronectin. They concluded that specific integrin receptor binding modulates downstream intracellular signaling pathways, including focal adhesion assembly and site-specific focal adhesion kinase (FAK) phosphorylation. FAK is related to cellular adhesion and drives osteoblast differentiation and mineralization. In another study, stem cells encapsulated in PEG hydrogels functionalized with phosphate- and t-butyl-groups led to osteogenic and adipogenic differentiation, respectively, without any growth factors [168]. Such tailored material chemistry can be implemented on 3D printed microfluidic surfaces for guided differentiation of stem cells under a dynamic environment [169].

Moreover, 3D printed native extracellular matrix components presents important chemical cues for guided stem cell differentiation. For example, calcium phosphate-based scaffolds have been used widely for bone regeneration from stem cells as they have chemical similarities to the inorganic component of bone [170]. Calcium phosphate scaffolds promote osteogenic differentiation of stem cells through the mitogen-activated protein kinase (MAPK) pathway (Fig. 12c) [171]. Activation of specific integrins through absorbed fibronectin and vitronectin on calcium phosphate scaffolds leads to focal contact formation and cytoskeleton reorganization. Integrin-mediated cell adhesion eventually triggers MAPK (ERK1/2 and p38) pathway directing MSC differentiation toward osteoblasts on calcium phosphate scaffolds. Moreover, endogenous factors like bone morphogenetic protein-2 (BMP-2) also partially control the osteogenic differentiation of stem cells on calcium phosphate scaffolds through BMP/Smad pathway [172]. Moreover, materials designed to bind to certain growth factors secreted by stem cells can amplify stem cell differentiation process to a specific lineage [173].

Mechanical stimulation is an important parameter for recapitulating some of the key aspects of tissues on a chip. Many reports suggest that such mechanical signals are transduced to biochemical signals, thereby controlling various biological processes such as ECM production, cellular proliferation, cell survival, and production of cytokines and chemokines [174, 175]. The multi-material capability of inkjet printers will be useful to incorporate mechanical stimulation in organs-on-chips. For example, flexible materials

can be used to fabricate a membrane actuated by pneumatic mechanism, and hard materials can be used to fabricate the physical structure of a microfluidic device [98]. Similarly, Stereolithography can also be used for fabricating a thin membrane-like layer upon which cells can be cultured under mechanical strain applied by pneumatic control channel (Fig. 12d(i)). Figure 12d(ii, iii) shows the front view of the device with cell-cultured on the top of the mechanically actuated membrane.

3D printable materials such as polyurethane, hydrogels, and silicones can be used for fabricating soft robots [176]. With their compliance, such soft-robots are being implemented in many biomedical applications such as prosthesis and rehabilitation devices, robotic surgery, drug delivery robots, and artificial organ development [177]. Such soft robotic actuators can be integrated with the heart to restore its function. In a recent study, a soft robotic system was integrated with cardiomyocytes in a microfluidic system to fabricate heart-on-a-chip (Fig. 12e(i–iii)) [178]. This cardiomyocyte driven system was capable of mimicking caterpillar motion and receiving chemical stimulus from isoproterenol drug. A higher concentration of isoproterenol drug increased myocardial contractile force and accelerated the crawling speed of soft robots in microfluidic tracks. Furthermore, the microfluidic system with soft robots was also stimulated with high potassium concentration (to simulate hyperkalemia disease), which stopped soft robotic motion in microfluidic tracks (Fig. 12e(iv,vi)). The motion was restored when a solution of potassium-ion and isoproterenol was introduced in the microfluidic gradient system Fig. 12e(v,vii)). The most effective drug concentration can be decided by observing the distance traveled by a soft robotic system. Thus, such soft robot integrated organ-on-a-chip can be an effective drug screening platform in the future.

With the introduction of novel biocompatible materials and multi-material high-resolution printers, 3D printing promises better recapitulation of various aspects of organs, including tissue architecture, spatial patterning of various cells, mechanical stimulation, vascularized networks, and other physiochemical properties on a microfluidic platform. Because of such advantages, we predict 3D printed organs-on-chips will be future 'hot-topic.' It will provide a reliable in vitro platform for organ modeling, disease modeling and possibly provide an alternative for in vivo drug testing models.

3D printed tumor-on-chips: toward personalized medicine

Conventional chemotherapy suggests a 'one-size-fits-all' approach for a particular cancer treatment [179]. However, the results of these treatment regimens vary from patient to patient with varying amounts of side-effects, often leading to treatment failure. One of the aims of developing tumor-on-a-chip platforms is to provide personalized treatment to cancer patients and minimize such side effects. Using minimal cell material from the biopsy sample, tumor-on-chips can help to decide the most effective treatment therapy. However, the results of drug testing on such platforms often generate large variations among the samples of the same patient due to the heterogeneity of tumor tissues, necessitating testing on multiple numbers of devices to predict statistically accurate drug effects [138, 180, 181]. 3D printing can effectively fabricate such platforms in bulk with less time consumption to predict the anti-cancer drug response accurately. Currently, spheroid-based and tumor tissue-based models have been successfully 3D printed for drug testing.

Beckwith et al. 3D printed a tumor trapping microfluidic device from Pro3dure GR-10 resin (Fig. 13a) [115]. This platform was able to retain the tissue fragment alive for at least 72 h and monitor the effect of immunotherapeutic agents. They cultured lung tumor biopsy samples and treated them with anti-PD-1, which led to the death of tumor cells because of the resident T cells activity [138]. Figure 13b shows a stained tumor tissue in the tumor trapping zone. Such 3D printed platforms can be rapidly 3D printed in clinical settings to culture patient-specific tumors, allowing simultaneous samples testing with various drug combinations to design effective and personalized immunotherapy treatment.

Yi et al. 3D printed glioblastoma-on-a-chip using endothelial cells and patient-derived glioblastoma cells [182]. The cells were encapsulated in decellularized porcine brain ink. The model recapitulated three distinct oxygen gradient regions with compartmentalized cancer-stroma structure and brain-ECM environment found in the native glioblastoma environment. Moreover, this model can be used to identify potential drug combinations based on patient-derived cells.

Fang et al. cultured gradient-sized spheroids in agarose wells fabricated by stereolithography mold and investigated drug penetration dependency on spheroid size [117]. Figure 13c shows a 3D printed template for the fabrication of agarose wells. The device works on the principle of surface tension wherein a droplet of cell suspension forms a liquid dome allowing variable numbers of cells to settle at the bottom of the wells, thereby forming gradient-sized spheroids (Fig. 13d). Similarly, stereolithography molds have also been used to fabricate microfluidic devices for generating uniform-sized spheroids [118]. Such platforms can culture a large number of patient-derived spheroids and evaluate the drug response for providing personalized treatment.

With the low-cost and rapid fabrication ability, 3D printing will enhance the applicability of tumor-on-chips in clinical settings and pave the way for providing personalized and precision medicine to cancer patients.

With the ease of fabricating in vitro microfluidic platforms, researchers will tend to use 3D printed microfluidic

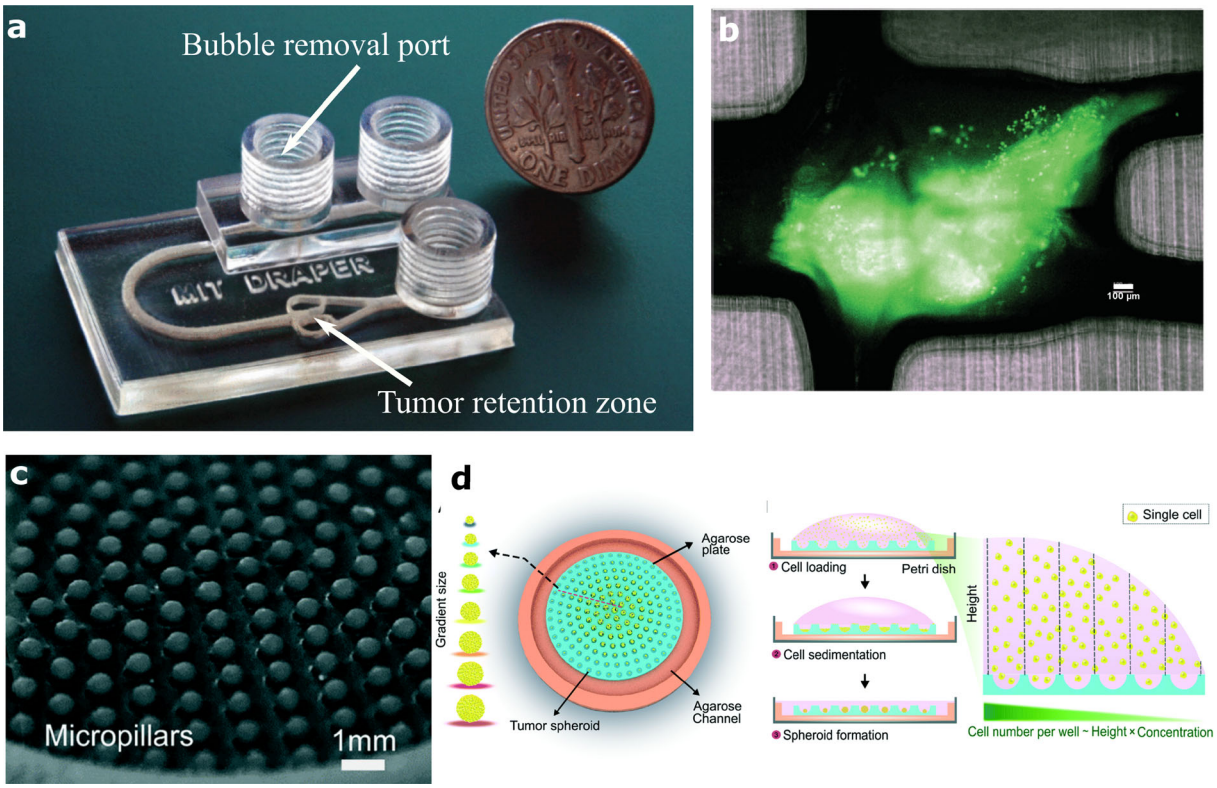

Fig. 13 3D printed tumor-on-chips (**a**) 3D printed tumor trapping microfluidic device. (**b**) Trapped tumor fragment. (**c**) Micropillars on a 3D printed mold for fabricating agarose wells. (**d**) Working principle of the spheroids forming chip with a gradient in size. Panels (**a**) and (**b**) are reproduced from [115] under the Creative Commons Attribution 4.0 International Public License (https://creativecommons.org/licenses/by/4.0/). A scale bar has been added with larger font size in (**b**). Panels (**c**) and (**d**) are reproduced from Ref. [117] with permission from The Royal Society of Chemistry

models over conventional non-microfluidic 2D/3D models for disease modeling, organ modeling, cancer drug testing, and cancer modeling.

Conclusion

There has been a growing interest in manufacturing microfluidic devices using 3D printing because of the rapid and simplified fabrication process. This is the first time a review provided a detailed discussion on fundamental manufacturing approaches in 3D printing used to fabricate microfluidic devices. From the four fundamental approaches, we found the mold-based approach is the most feasible way of implementing 3D printing technologies for fabricating microfluidic devices. It does not involve the direct use of unknown 3D printing materials and works on a similar principle as soft lithography. 3D printed microfluidic devices have been implemented in various fields, including chemical, biological, and material synthesis. We have discussed some of the crucial challenges related to 3D printing of microfluidic devices and how the recent research progress in 3D printing materials and fundamental approaches aided in overcoming them. Lastly, we have outlined possible implications of 3D printed microfluidics on the fields of healthcare such as disease modeling, novel drug development, organ modeling, personalized treatment for cancer, and cancer drug screening by discussing the current state and future outlook of 3D printed 'organs-on-chips,' and 3D printed 'tumor-on-chips.' We can expect rapid development of physiologically relevant organs-on-chips by 3D printing, which will aid in disease modeling, organ modeling and possibly provide an alternative for in vivo drug testing models.

Similarly, 3D printed 'tumor-on-chips' will be fabricated readily in clinical settings to provide effective personalized treatment to cancer patients. Although 3D printing has advanced significantly in terms of resolution, the properties of 3D printable materials are still inferior to PDMS, which suggests a need for further research in the material aspects of 3D printing. We believe multi-material organs-on-chips, 3D printed tumor-on-chips, development of commercial low-cost and high-resolution printers, novel biocompatible materials for 3D printing, optically transparent materials with high absorbance properties, materials with high gas perme-

ability, materials with low autofluorescence, and materials compatible with autoclave sterilization will be some of the future research directions in the field of 3D printed microfluidics.

Acknowledgements This work was supported by the Prime Minister's Research Fellowship (PMRF) provided by the Ministry of Human Resource Development (MHRD, Govt. of India). We thank Sukanya V S for her valuable suggestions to improve the manuscript.

Author contributions VM was involved in conceptualization, writing—original draft, and visualization; VM and SNR helped in writing—review & editing; and SNR contributed to supervision.

Compliance with ethical standards

Conflict of interest The authors declare that there is no conflict of interest.

Ethical approval This study does not contain any studies with human or animal subjects performed by any of the authors.

References

1. Chung S, Sudo R, Vickerman V, Zervantonakis IK, Kamm RD (2010) Microfluidic platforms for studies of angiogenesis, cell migration, and cell-cell interactions: sixth international biofluid mechanics symposium and workshop March 28–30, 2008 Pasadena, California. Ann Biomed Eng 38:1164–1177. https://doi.org/10.1007/s10439-010-9899-3
2. Jeong GS, Han S, Shin Y, Kwon GH, Kamm RD, Lee SH, Chung S (2011) Sprouting angiogenesis under a chemical gradient regulated by interactions with an endothelial monolayer in a microfluidic platform. Anal Chem 83:8454–8459. https://doi.org/10.1021/ac202170e
3. Bein A, Shin W, Jalili-Firoozinezhad S, Park MH, Sontheimer-Phelps A, Tovaglieri A, Chalkiadaki A, Kim HJ, Ingber DE (2018) Microfluidic organ-on-a-chip models of human intestine. CMGH 5:659–668. https://doi.org/10.1016/j.jcmgh.2017.12.010
4. Huh D (2015) A human breathing lung-on-a-chip. In: Annals of the American Thoracic Society. American Thoracic Society, pp S42–S44
5. Huh D, Torisawa YS, Hamilton GA, Kim HJ, Ingber DE (2012) Microengineered physiological biomimicry: organs-on-chips. Lab Chip 12:2156–2164. https://doi.org/10.1039/c2lc40089h
6. Zhu J (2020) Application of organ-on-chip in drug discovery. J Biosci Med 08:119–134. https://doi.org/10.4236/jbm.2020.83011
7. Herland A, Maoz BM, Das D, Somayaji MR, Prantil-Baun R, Novak R, Cronce M, Huffstater T, Jeanty SSF, Ingram M, Chalkiadaki A, Benson Chou D, Marquez S, Delahanty A, Jalili-Firoozinezhad S, Milton Y, Sontheimer-Phelps A, Swenor B, Levy O, Parker KK, Przekwas A, Ingber DE (2020) Quantitative prediction of human pharmacokinetic responses to drugs via fluidically coupled vascularized organ chips. Nat Biomed Eng 4:421–436. https://doi.org/10.1038/s41551-019-0498-9
8. Lin H, Lozito TP, Alexander PG, Gottardi R, Tuan RS (2014) Stem cell-based microphysiological osteochondral system to model tissue response to interleukin-1B. Mol Pharm 11:2203–2212. https://doi.org/10.1021/mp500136b
9. Tsai HF, Trubelja A, Shen AQ, Bao G (2017) Tumour-on-a-chip: Microfluidic models of tumour morphology, growth and microenvironment. J R Soc Interface 14:20170137. https://doi.org/10.1098/rsif.2017.0137
10. Ma Y-HV, Middleton K, You L, Sun Y (2018) A review of microfluidic approaches for investigating cancer extravasation during metastasis. Microsyst Nanoeng 4:1–13. https://doi.org/10.1038/micronano.2017.104
11. Dhiman N, Kingshott P, Sumer H, Sharma CS, Rath SN (2019) On-chip anticancer drug screening—recent progress in microfluidic platforms to address challenges in chemotherapy. Biosens Bioelectron 137:236–254. https://doi.org/10.1016/j.bios.2019.02.070
12. Dhiman N, Shagaghi N, Bhave M, Sumer H, Kingshott P, Rath SN (2020) Selective cytotoxicity of a novel Trp-rich peptide against lung tumor spheroids encapsulated inside a 3D microfluidic device. Adv Biosyst 4:1900285. https://doi.org/10.1002/adbi.201900285
13. Sankar S, Kakunuri MD, EswaramoorthySharmaRath SCSSN (2018) Effect of patterned electrospun hierarchical structures on alignment and differentiation of mesenchymal stem cells: biomimicking bone. J Tissue Eng Regen Med 12:2073–2084. https://doi.org/10.1002/term.2640
14. Qin D, Xia Y, Whitesides GM (2010) Soft lithography for micro- and nanoscale patterning. Nat Protoc 5:491–502. https://doi.org/10.1038/nprot.2009.234
15. Shin Y, Han S, Jeon JS, Yamamoto K, Zervantonakis IK, Sudo R, Kamm RD, Chung S (2012) Microfluidic assay for simultaneous culture of multiple cell types on surfaces or within hydrogels. Nat Protoc 7:1247–1259. https://doi.org/10.1038/nprot.2012.051
16. Sankar S, Sharma CS, Rath SN (2019) Enhanced osteodifferentiation of MSC spheroids on patterned electrospun fiber mats—an advanced 3D double strategy for bone tissue regeneration. Mater Sci Eng C 94:703–712. https://doi.org/10.1016/j.msec.2018.10.025
17. Bhattacharjee N, Urrios A, Kang S, Folch A (2016) The upcoming 3D-printing revolution in microfluidics. Lab Chip 16:1720–1742. https://doi.org/10.1039/c6lc00163g
18. Ho CMB, Ng SH, Li KHH, Yoon YJ (2015) 3D printed microfluidics for biological applications. Lab Chip 15:3627–3637. https://doi.org/10.1039/c5lc00685f
19. Chan HN, Chen Y, Shu Y, Chen Y, Tian Q, Wu H (2015) Direct, one-step molding of 3D-printed structures for convenient fabrication of truly 3D PDMS microfluidic chips. Microfluid Nanofluid 19:9–18. https://doi.org/10.1007/s10404-014-1542-4
20. Waheed S, Cabot JM, Macdonald NP, Lewis T, Guijt RM, Paull B, Breadmore MC (2016) 3D printed microfluidic devices: enablers and barriers. Lab Chip 16:1993–2013. https://doi.org/10.1039/c6lc00284f
21. Yazdi AA, Popma A, Wong W, Nguyen T, Pan Y, Xu J (2016) 3D printing: an emerging tool for novel microfluidics and lab-on-a-chip applications. Microfluid Nanofluid 20:1–18. https://doi.org/10.1007/s10404-016-1715-4
22. Naderi A, Bhattacharjee N, Folch A (2019) Digital manufacturing for microfluidics. Annu Rev Biomed Eng 21:325–364. https://doi.org/10.1146/annurev-bioeng-092618-020341
23. Weisgrab G, Ovsianikov A, Costa PF (2019) Functional 3D printing for microfluidic chips. Adv Mater Technol 4:1900275. https://doi.org/10.1002/admt.201900275
24. Waldbaur A, Rapp H, Länge K, Rapp BE (2011) Let there be chip—towards rapid prototyping of microfluidic devices: one-step manufacturing processes. Anal Methods 3:2681–2716. https://doi.org/10.1039/c1ay05253e
25. Chan HN, Tan MJA, Wu H (2017) Point-of-care testing: applications of 3D printing. Lab Chip 17:2713–2739. https://doi.org/10.1039/c7lc00397h

26. Au AK, Lee W, Folch A (2014) Mail-order microfluidics: evaluation of stereolithography for the production of microfluidic devices. Lab Chip 14:1294–1301. https://doi.org/10.1039/c3lc51360b
27. Shallan AI, Smejkal P, Corban M, Guijt RM, Breadmore MC (2014) Cost-effective three-dimensional printing of visibly transparent microchips within minutes. Anal Chem 86:3124–3130. https://doi.org/10.1021/ac4041857
28. Nelson MD, Ramkumar N, Gale BK (2019) Flexible, transparent, sub-100 μm microfluidic channels with fused deposition modeling 3D-printed thermoplastic polyurethane. J Micromech Microeng 29:095010. https://doi.org/10.1088/1361-6439/AB2F26
29. Bhargava KC, Thompson B, Malmstadt N (2014) Discrete elements for 3D microfluidics. Proc Natl Acad Sci 111:15013–15018. https://doi.org/10.1073/pnas.1414764111
30. Rhee M, Burns MA (2008) Microfluidic assembly blocks. Lab Chip 8:1365–1373. https://doi.org/10.1039/b805137b
31. Langelier SM, Livak-Dahl E, Manzo AJ, Johnson BN, Walter NG, Burns MA (2011) Flexible casting of modular self-aligning microfluidic assembly blocks. Lab Chip 11:1679–1687. https://doi.org/10.1039/c0lc00517g
32. Grodzinski P, Yang J, Liu RH, Ward MD (2003) A modular microfluidic system for cell pre-concentration and genetic sample preparation. Biomed Microdev 5:303–310. https://doi.org/10.1023/A:1027357713526
33. Sun K, Wang Z, Jiang X (2008) Modular microfluidics for gradient generation. Lab Chip 8:1536–1543. https://doi.org/10.1039/b806140h
34. Yuen PK (2008) SmartBuild—a truly plug-n-play modular microfluidic system. Lab Chip 8:1374–1378. https://doi.org/10.1039/b805086d
35. Vittayarukskul K, Lee AP (2017) A truly Lego®-like modular microfluidics platform. J Micromech Microeng 27:035004. https://doi.org/10.1088/1361-6439/AA53ED
36. Bressan LP, Adamo CB, Quero RF, De Jesus DP, Da Silva JAF (2019) A simple procedure to produce FDM-based 3D-printed microfluidic devices with an integrated PMMA optical window. Anal Methods 11:1014–1020. https://doi.org/10.1039/c8ay02092b
37. Cheon J, Kim S (2019) Intermediate layer-based bonding techniques for polydimethylsiloxane/digital light processing 3D-printed microfluidic devices. J Micromech Microeng 29:095005. https://doi.org/10.1088/1361-6439/ab27d3
38. Brennan MD, Rexius-Hall ML, Eddington DT (2015) A 3D-printed oxygen control insert for a 24-well plate. PLoS ONE 10:e0137631. https://doi.org/10.1371/journal.pone.0137631
39. Lee H, Cho DW (2016) One-step fabrication of an organ-on-a-chip with spatial heterogeneity using a 3D bioprinting technology. Lab Chip 16:2618–2625. https://doi.org/10.1039/c6lc00450d
40. Mehta G, Lee J, Cha W, Tung YC, Linderman JJ, Takayama S (2009) Hard top soft bottom microfluidic devices for cell culture and chemical analysis. Anal Chem 81:3714–3722. https://doi.org/10.1021/ac802178u
41. Pranzo D, Larizza P, Filippini D, Percoco G (2018) Extrusion-based 3D printing of microfluidic devices for chemical and biomedical applications: a topical review. Micromachines. https://doi.org/10.3390/mi9080374
42. Gu Z, Fu J, Lin H, He Y (2019) Development of 3D bioprinting: from printing methods to biomedical applications. Asian J Pharm Sci. https://doi.org/10.1016/j.ajps.2019.11.003
43. Ozbolat IT, Hospodiuk M (2016) Current advances and future perspectives in extrusion-based bioprinting. Biomaterials 76:321–343. https://doi.org/10.1016/j.biomaterials.2015.10.076
44. Hölzl K, Lin S, Tytgat L, Van Vlierberghe S, Gu L, Ovsianikov A (2016) Bioink properties before, during and after 3D bioprinting. Biofabrication 8:032002. https://doi.org/10.1088/1758-5090/8/3/032002
45. Romanov V, Samuel R, Chaharlang M, Jafek AR, Frost A, Gale BK (2018) FDM 3D printing of high-pressure, heat-resistant, transparent microfluidic devices. Anal Chem 90:10450–10456. https://doi.org/10.1021/acs.analchem.8b02356
46. Kitson PJ, Symes MD, Dragone V, Cronin L (2013) Combining 3D printing and liquid handling to produce user-friendly reactionware for chemical synthesis and purification. Chem Sci 4:3099–3103. https://doi.org/10.1039/c3sc51253c
47. Kitson PJ, Rosnes MH, Sans V, Dragone V, Cronin L (2012) Configurable 3D-printed millifluidic and microfluidic "lab on a chip" reactionware devices. Lab Chip 12:3267–3271. https://doi.org/10.1039/c2lc40761b
48. Yuen PK (2016) Embedding objects during 3D printing to add new functionalities. Biomicrofluidics 10:044104. https://doi.org/10.1063/1.4958909
49. Gaal G, Mendes M, de Almeida TP, Piazzetta MHO, Gobbi ÂL, Riul A, Rodrigues V (2017) Simplified fabrication of integrated microfluidic devices using fused deposition modeling 3D printing. Sens Actuators B Chem 242:35–40. https://doi.org/10.1016/j.snb.2016.10.110
50. Li F, Smejkal P, Macdonald NP, Guijt RM, Breadmore MC (2017) One-step fabrication of a microfluidic device with an integrated membrane and embedded reagents by multimaterial 3D printing. Anal Chem 89:4701–4707. https://doi.org/10.1021/acs.analchem.7b00409
51. Bressan LP, Lima TM, da Silveira GD, da Silva JAF (2020) Low-cost and simple FDM-based 3D-printed microfluidic device for the synthesis of metallic core–shell nanoparticles. SN Appl Sci 2:1–8. https://doi.org/10.1007/s42452-020-2768-2
52. Salentijn GIJ, Oomen PE, Grajewski M, Verpoorte E (2017) Fused deposition modeling 3D printing for (bio)analytical device fabrication: procedures, materials, and applications. Anal Chem 89:7053–7061. https://doi.org/10.1021/acs.analchem.7b00828
53. Ye J, Chu T, Chu J, Gao B, He B (2019) A versatile approach for enzyme immobilization using chemically modified 3D-printed scaffolds. ACS Sustain Chem Eng 7:18048–18054. https://doi.org/10.1021/acssuschemeng.9b04980
54. Saggiomo V, Velders AH (2015) Simple 3D printed scaffold-removal method for the fabrication of intricate microfluidic devices. Adv Sci 2:1500125. https://doi.org/10.1002/advs.201500125
55. Tang W, Fan N, Yang J, Li Z, Zhu L, Jiang D, Shi J, Xiang N (2019) Elasto-inertial particle focusing in 3D-printed microchannels with unconventional cross sections. Microfluid Nanofluid 23:42. https://doi.org/10.1007/s10404-019-2205-2
56. Goh WH, Hashimoto M (2018a) Fabrication of 3D microfluidic channels and in-channel features using 3D printed, water-soluble sacrificial mold. Macromol Mater Eng 303:1700484. https://doi.org/10.1002/mame.201700484
57. Goh W, Hashimoto M (2018b) Dual sacrificial molding: fabricating 3D microchannels with overhang and helical features. Micromachines 9:523. https://doi.org/10.3390/mi9100523
58. Shankles PG, Millet LJ, Aufrecht JA, Retterer ST (2018) Accessing microfluidics through feature-based design software for 3D printing. PLoS One 13:e0192752. https://doi.org/10.1371/journal.pone.0192752
59. Morgan AJL, San Jose LH, Jamieson WD, Wymant JM, Song B, Stephens P, Barrow DA, Castell OK (2016) Simple and versatile 3D printed microfluidics using fused filament fabrication. PLoS ONE 11:e0152023. https://doi.org/10.1371/journal.pone.0152023
60. Tsuda S, Jaffery H, Doran D, Hezwani M, Robbins PJ, Yoshida M, Cronin L (2015) Customizable 3D printed 'plug and play' milliflu-

idic devices for programmable fluidics. PLoS One 10:e0141640. https://doi.org/10.1371/journal.pone.0141640
61. Nie J, Gao Q, Qiu JJ, Sun M, Liu A, Shao L, Fu JZ, Zhao P, He Y (2018) 3D printed Lego® -like modular microfluidic devices based on capillary driving. Biofabrication 10:035001. https://doi.org/10.1088/1758-5090/aaadd3
62. Ching T, Li Y, Karyappa R, Ohno A, Toh YC, Hashimoto M (2019) Fabrication of integrated microfluidic devices by direct ink writing (DIW) 3D printing. Sens Actuators B Chem 297:126609. https://doi.org/10.1016/j.snb.2019.05.086
63. Johnson BN, Lancaster KZ, Hogue IB, Meng F, Kong YL, Enquist LW, McAlpine MC (2016) 3D printed nervous system on a chip. Lab Chip 16:1393–1400. https://doi.org/10.1039/c5lc01270h
64. Therriault D, White SR, Lewis JA (2003) Chaotic mixing in three-dimensional microvascular networks fabricated by direct-write assembly. Nat Mater 2:265–271. https://doi.org/10.1038/nmat863
65. Toohey KS, Sottos NR, Lewis JA, Moore JS, White SR (2007) Self-healing materials with microvascular networks. Nat Mater 6:581–585. https://doi.org/10.1038/nmat1934
66. He Y, Qiu J, Fu J, Zhang J, Ren Y, Liu A (2015) Printing 3D microfluidic chips with a 3D sugar printer. Microfluid Nanofluidics 19:447–456. https://doi.org/10.1007/s10404-015-1571-7
67. Miller JS, Stevens KR, Yang MT, Baker BM, Nguyen DHT, Cohen DM, Toro E, Chen AA, Galie PA, Yu X, Chaturvedi R, Bhatia SN, Chen CS (2012) Rapid casting of patterned vascular networks for perfusable engineered three-dimensional tissues. Nat Mater 11:768–774. https://doi.org/10.1038/nmat3357
68. Gelber MK, Bhargava R (2015) Monolithic multilayer microfluidics via sacrificial molding of 3D-printed isomalt. Lab Chip 15:1736–1741. https://doi.org/10.1039/c4lc01392a
69. Wu W, DeConinck A, Lewis JA (2011) Omnidirectional printing of 3D microvascular networks. Adv Mater 23:H178–H183. https://doi.org/10.1002/adma.201004625
70. Kolesky DB, Truby RL, Gladman AS, Busbee TA, Homan KA, Lewis JA (2014) 3D Bioprinting of vascularized, heterogeneous cell-laden tissue constructs. Adv Mater 26:3124–3130. https://doi.org/10.1002/adma.201305506
71. Bertassoni LE, Cecconi M, Manoharan V, Nikkhah M, Hjortnaes J, Cristino AL, Barabaschi G, Demarchi D, Dokmeci MR, Yang Y, Khademhosseini A (2014) Hydrogel bioprinted microchannel networks for vascularization of tissue engineering constructs. Lab Chip 14:2202–2211. https://doi.org/10.1039/c4lc00030g
72. Formlabs.com SLA vs. DLP: Guide to Resin 3D Printers | Formlabs. https://formlabs.com/blog/resin-3d-printer-comparison-sla-vs-dlp/. Accessed 9 Apr 2020
73. Urrios A, Parra-Cabrera C, Bhattacharjee N, Gonzalez-Suarez AM, Rigat-Brugarolas LG, Nallapatti U, Samitier J, Deforest CA, Posas F, Garcia-Cordero JL, Folch A (2016) 3D-printing of transparent bio-microfluidic devices in PEG-DA. Lab Chip 16:2287–2294. https://doi.org/10.1039/c6lc00153j
74. Kuo AP, Bhattacharjee N, Lee YS, Castro K, Kim YT, Folch A (2019) High-precision stereolithography of biomicrofluidic devices. Adv Mater Technol 4:1–11. https://doi.org/10.1002/admt.201800395
75. Kim YT, Bohjanen S, Bhattacharjee N, Folch A (2019) Partitioning of hydrogels in 3D-printed microchannels. Lab Chip 19:3086–3093. https://doi.org/10.1039/c9lc00535h
76. Gong H, Bickham BP, Woolley AT, Nordin GP (2017) Custom 3D printer and resin for 18 μm × 20 μm microfluidic flow channels. Lab Chip 17:2899–2909. https://doi.org/10.1039/c7lc00644f
77. Bhattacharjee N, Parra-Cabrera C, Kim YT, Kuo AP, Folch A (2018) Desktop-stereolithography 3D-printing of a poly(dimethylsiloxane)-based material with sylgard-184 properties. Adv Mater 30:1–7. https://doi.org/10.1002/adma.201800001
78. Au AK, Bhattacharjee N, Horowitz LF, Chang TC, Folch A (2015) 3D-printed microfluidic automation. Lab Chip 15:1934–1941. https://doi.org/10.1039/c5lc00126a
79. Rogers CI, Qaderi K, Woolley AT, Nordin GP (2015) 3D printed microfluidic devices with integrated valves. Biomicrofluidics 9:016501. https://doi.org/10.1063/1.4905840
80. Chen Z, Han JY, Shumate L, Fedak R, DeVoe DL (2019) High throughput nanoliposome formation using 3D printed microfluidic flow focusing chips. Adv Mater Technol 4:1800511. https://doi.org/10.1002/admt.201800511
81. Kamperman T, Teixeira LM, Salehi SS, Kerckhofs G, Guyot Y, Geven M, Geris L, Grijpma D, Blanquer S, Leijten J (2020) Engineering 3D parallelized microfluidic droplet generators with equal flow profiles by computational fluid dynamics and stereolithographic printing. Lab Chip 20:490–495. https://doi.org/10.1039/c9lc00980a
82. Chiadò A, Palmara G, Chiappone A, Tanzanu C, Pirri CF, Roppolo I, Frascella F (2020) A modular 3D printed lab-on-a-chip for early cancer detection. Lab Chip 20:665–674. https://doi.org/10.1039/c9lc01108k
83. Nichols DA, Sondh IS, Litte SR, Zunino P, Gottardi R (2018) Design and validation of an osteochondral bioreactor for the screening of treatments for osteoarthritis. Biomed Microdev. https://doi.org/10.1007/s10544-018-0264-x
84. Knowlton S, Yu CH, Ersoy F, Emadi S, Khademhosseini A, Tasoglu S (2016) 3D-printed microfluidic chips with patterned, cell-laden hydrogel constructs. Biofabrication 8:1–13. https://doi.org/10.1088/1758-5090/8/2/025019
85. Ong LJY, Islam A, Dasgupta R, Iyer NG, Leo HL, Toh YC (2017) A 3D printed microfluidic perfusion device for multicellular spheroid cultures. Biofabrication 9:045005. https://doi.org/10.1088/1758-5090/aa8858
86. Comina G, Suska A, Filippini D (2014) PDMS lab-on-a-chip fabrication using 3D printed templates. Lab Chip 14:424–430. https://doi.org/10.1039/c3lc50956g
87. Razavi Bazaz S, Kashaninejad N, Azadi S, Patel K, Asadnia M, Jin D, Ebrahimi Warkiani M (2019) Rapid soft lithography using 3D-printed molds. Adv Mater Technol 4:1900425. https://doi.org/10.1002/admt.201900425
88. Hernández Vera R, O'Callaghan P, Fatsis-Kavalopoulos N, Kreuger J (2019) Modular microfluidic systems cast from 3D-printed molds for imaging leukocyte adherence to differentially treated endothelial cultures. Sci Rep. https://doi.org/10.1038/s41598-019-47475-z
89. Mohamed M, Kumar H, Wang Z, Martin N, Mills B, Kim K (2019) Rapid and inexpensive fabrication of multi-depth microfluidic device using high-resolution LCD stereolithographic 3D printing. J Manuf Mater Process 3:26. https://doi.org/10.3390/jmmp3010026
90. Ching T, Toh YC, Hashimoto M (2020) Fabrication of complex 3D fluidic networks via modularized stereolithography. Adv Eng Mater 22:1901109. https://doi.org/10.1002/adem.201901109
91. Custompart.net Jetted Photopolymer. http://www.custompartnet.com/wu/jetted-photopolymer. Accessed 8 Apr 2020
92. Facfox PolyJet vs MultiJet Printing(MJP)—FacFox. https://facfox.com/docs/polyjet-mjp-comparison. Accessed 8 Apr 2020
93. 3dsystems Our Story | 3D Systems. https://www.3dsystems.com/our-story. Accessed 8 Apr 2020
94. Enders A, Siller IG, Urmann K, Hoffmann MR, Bahnemann J (2019) 3D printed microfluidic mixers—a comparative study on mixing unit performances. Small 15:1804326. https://doi.org/10.1002/smll.201804326
95. Anderson KB, Lockwood SY, Martin RS, Spence DM (2013) A 3D printed fluidic device that enables integrated features. Anal Chem 85:5622–5626. https://doi.org/10.1021/ac4009594

96. Barbaresco F, Cocuzza M, Pirri CF, Marasso SL (2020) Application of a micro free-flow electrophoresis 3D printed lab-on-a-chip for micro-nanoparticles analysis. Nanomaterials 10:1277. https://doi.org/10.3390/nano10071277
97. Ji Q, Zhang JM, Liu Y, Li X, Lv P, Jin D, Duan H (2018) A modular microfluidic device via multimaterial 3D printing for emulsion generation. Sci Rep 8:1–11. https://doi.org/10.1038/s41598-018-22756-1
98. Keating SJ, Gariboldi MI, Patrick WG, Sharma S, Kong DS, Oxman N (2016) 3D printed multimaterial microfluidic valve. PLoS One 11:e0160624. https://doi.org/10.1371/journal.pone.0160624
99. IchiroMashimoKoyamaFockenbergNakashimaNakajimaLiChen KKYYCMMJY (2015) 3D printing of soft lithography mold for rapid production of polydimethylsiloxane-based microfluidic devices for cell stimulation with concentration gradients. Biomed Microdev 17:36. https://doi.org/10.1007/s10544-015-9928-y
100. Glick CC, Srimongkol MT, Schwartz AJ, Zhuang WS, Lin JC, Warren RH, Tekell DR, Satamalee PA, Lin L (2016) Rapid assembly of multilayer microfluidic structures via 3D-printed transfer molding and bonding. Microsystems Nanoeng 2:1–9. https://doi.org/10.1038/micronano.2016.63
101. Brossard R, Brouchet T, Malloggi F (2019) Replication of a printed volatile mold: a novel microfabrication method for advanced microfluidic systems. Sci Rep 9:1–10. https://doi.org/10.1038/s41598-019-53729-7
102. Hwang Y, Paydar OH, Candler RN (2015) 3D printed molds for non-planar PDMS microfluidic channels. Sens Actuators A Phys 226:137–142. https://doi.org/10.1016/j.sna.2015.02.028
103. Li Z, Yang J, Li K, Zhu L, Tang W (2017) Fabrication of PDMS microfluidic devices with 3D wax jetting. RSC Adv 7:3313–3320. https://doi.org/10.1039/C6RA24884E
104. Sunkara V, Park DK, Hwang H, Chantiwas R, Soper SA, Cho YK (2011) Simple room temperature bonding of thermoplastics and poly(dimethylsiloxane). Lab Chip 11:962–965. https://doi.org/10.1039/c0lc00272k
105. Ahn SY, Lee NY (2015) Solvent-free thermoplastic-poly(dimethylsiloxane) bonding mediated by UV irradiation followed by gas-phase chemical deposition of an adhesion linker. J Micromech Microeng 25:075007. https://doi.org/10.1088/0960-1317/25/7/075007
106. Kim K, Park SW, Yang SS (2010) The optimization of PDMS-PMMA bonding process using silane primer. Biochip J 4:148–154. https://doi.org/10.1007/s13206-010-4210-0
107. Vlachopoulou ME, Tserepi A, Pavli P, Argitis P, Sanopoulou M, Misiakos K (2009) A low temperature surface modification assisted method for bonding plastic substrates. J Micromech Microeng 19:015007. https://doi.org/10.1088/0960-1317/19/1/015007
108. Tang L, Lee NY (2010) A facile route for irreversible bonding of plastic-PDMS hybrid microdevices at room temperature. Lab Chip 10:1274–1280. https://doi.org/10.1039/b924753j
109. Tsao CW, Hromada L, Liu J, Kumar P, DeVoe DL (2007) Low temperature bonding of PMMA and COC microfluidic substrates using UV/ozone surface treatment. Lab Chip 7:499–505. https://doi.org/10.1039/b618901f
110. Duong LH, Chen PC (2019) Simple and low-cost production of hybrid 3D-printed microfluidic devices. Biomicrofluidics 13:024108. https://doi.org/10.1063/1.5092529
111. Lynh HD, Pin-Chuan C (2018) Novel solvent bonding method for creation of a three-dimensional, non-planar, hybrid PLA/PMMA microfluidic chip. Sens Actuators A Phys 280:350–358. https://doi.org/10.1016/j.sna.2018.08.002
112. Bressan LP, Robles-Najar J, Adamo CB, Quero RF, Costa BMC, de Jesus DP, da Silva JAF (2019) 3D-printed microfluidic device for the synthesis of silver and gold nanoparticles. Microchem J 146:1083–1089. https://doi.org/10.1016/j.microc.2019.02.043
113. Kecili S, Tekin HC (2020) Adhesive bonding strategies to fabricate high-strength and transparent 3D printed microfluidic device. Biomicrofluidics 14:024113. https://doi.org/10.1063/5.0003302
114. Carrell CS, McCord CP, Wydallis RM, Henry CS (2020) Sealing 3D-printed parts to poly(dimethylsiloxane) for simple fabrication of microfluidic devices. Anal Chim Acta 1124:78–84. https://doi.org/10.1016/j.aca.2020.05.014
115. Beckwith AL, Borenstein JT, Velasquez-Garcia LF (2018) Monolithic, 3D-printed microfluidic platform for recapitulation of dynamic tumor microenvironments. J Microelectromech Syst 27:1009–1022. https://doi.org/10.1109/JMEMS.2018.2869327
116. Shrestha J, Ghadiri M, Shanmugavel M, Bazaz SR, Vasilescu S, Ding L, Warkiani ME (2020) A rapidly prototyped lung-on-a-chip model using 3D-printed molds. Organs-on-a-Chip 1:100001. https://doi.org/10.1016/j.ooc.2020.100001
117. Fang G, Lu H, Law A, Gallego-Ortega D, Jin D, Lin G (2019) Gradient-sized control of tumor spheroids on a single chip. Lab Chip 19:4093–4103. https://doi.org/10.1039/c9lc00872a
118. Ruppen J, Wildhaber FD, Strub C, Hall SRR, Schmid RA, Geiser T, Guenat OT (2015) Towards personalized medicine: chemosensitivity assays of patient lung cancer cell spheroids in a perfused microfluidic platform. Lab Chip 15:3076–3085. https://doi.org/10.1039/c5lc00454c
119. Ukita Y, Takamura Y, Utsumi Y (2016) Direct digital manufacturing of autonomous centrifugal microfluidic device. In: Japanese Journal of Applied Physics. Japan Society of Applied Physics, p 06GN02
120. Gong H, Beauchamp M, Perry S, Woolley AT, Nordin GP (2015) Optical approach to resin formulation for 3D printed microfluidics. RSC Adv 5:106621–106632. https://doi.org/10.1039/c5ra23855b
121. Grigoryan B, Paulsen SJ, Corbett DC, Sazer DW, Fortin CL, Zaita AJ, Greenfield PT, Calafat NJ, Gounley JP, Ta AH, Johansson F, Randles A, Rosenkrantz JE, Louis-Rosenberg JD, Galie PA, Stevens KR, Miller JS (2019) Multivascular networks and functional intravascular topologies within biocompatible hydrogels. Science (80-) 364:458–464. https://doi.org/10.1126/science.aav9750
122. Tothill AM, Partridge M, James SW, Tatam RP (2017) Fabrication and optimisation of a fused filament 3D-printed microfluidic platform. J Micromech Microeng 27:035018. https://doi.org/10.1088/1361-6439/AA5AE3
123. Zhu F, Friedrich T, Nugegoda D, Kaslin J, Wlodkowic D (2015) Assessment of the biocompatibility of three-dimensional-printed polymers using multispecies toxicity tests. Biomicrofluidics 9:061103. https://doi.org/10.1063/1.4939031
124. Rimington RP, Capel AJ, Christie SDR, Lewis MP (2017) Biocompatible 3D printed polymers: via fused deposition modelling direct C2C12 cellular phenotype in vitro. Lab Chip 17:2982–2993. https://doi.org/10.1039/c7lc00577f
125. de Almeida Monteiro Melo FerrazNagashimaVenzacLe Gac-Songsasen MJBBSN (2020) 3D printed mold leachates in PDMS microfluidic devices. Sci Rep 10:1–9. https://doi.org/10.1038/s41598-020-57816-y
126. Gross BC, Anderson KB, Meisel JE, McNitt MI, Spence DM (2015) Polymer coatings in 3D-printed fluidic device channels for improved cellular adherence prior to electrical lysis. Anal Chem 87:6335–6341. https://doi.org/10.1021/acs.analchem.5b01202
127. MacDonald NP, Zhu F, Hall CJ, Reboud J, Crosier PS, Patton EE, Wlodkowic D, Cooper JM (2016) Assessment of biocompatibility of 3D printed photopolymers using zebrafish embryo toxicity assays. Lab Chip 16:291–297. https://doi.org/10.1039/c5lc01374g

128. Leonhardt S, Klare M, Scheer M, Fischer T, Cordes B, Eblenkamp M (2016) Biocompatibility of photopolymers for additive manufacturing. Curr Dir Biomed Eng. https://doi.org/10.1515/cdbme-2016-0028
129. Macdonald NP, Cabot JM, Smejkal P, Guijt RM, Paull B, Breadmore MC (2017) Comparing microfluidic performance of three-dimensional (3D) printing platforms. Anal Chem 89:3858–3866. https://doi.org/10.1021/acs.analchem.7b00136
130. Armstrong C Post processing for FDM printed parts | 3D Hubs. https://www.3dhubs.com/knowledge-base/post-processing-fdm-printed-parts/. Accessed 30 Apr 2020
131. Lalehpour A, Janeteas C, Barari A (2018) Surface roughness of FDM parts after post-processing with acetone vapor bath smoothing process. Int J Adv Manuf Technol 95:1505–1520. https://doi.org/10.1007/s00170-017-1165-5
132. Villegas M, Cetinic Z, Shakeri A, Didar TF (2018) Fabricating smooth PDMS microfluidic channels from low-resolution 3D printed molds using an omniphobic lubricant-infused coating. Anal Chim Acta 1000:248–255. https://doi.org/10.1016/j.aca.2017.11.063
133. Van Midwoud PM, Janse A, Merema MT, Groothuis GMM, Verpoorte E (2012) Comparison of biocompatibility and adsorption properties of different plastics for advanced microfluidic cell and tissue culture models. Anal Chem 84:3938–3944. https://doi.org/10.1021/ac300771z
134. Özçam AE, Efimenko K, Genzer J (2014) Effect of ultraviolet/ozone treatment on the surface and bulk properties of poly(dimethyl siloxane) and poly(vinylmethyl siloxane) networks. Polymer (Guildf) 55:3107–3119. https://doi.org/10.1016/j.polymer.2014.05.027
135. Wilhelm E, Neumann C, Sachsenheimer K, Schmitt T, Länge K, Rapp BE (2013) Rapid bonding of polydimethylsiloxane to stereolithographically manufactured epoxy components using a photogenerated intermediary layer. Lab Chip 13:2268–2271. https://doi.org/10.1039/c3lc50341k
136. Perez M, Block M, Espalin D, Winker R, Hoppe T, Medina F, Wicker R (2012) Sterilization of fdm-manufactured parts. In: 23rd annual international solid freeform fabrication symposium—an additive manufacturing conference, SFF 2012. pp 285–296
137. Walleser M Sterile 3D Printing for Medical Applications and Sterile Outcomes. https://blog.gotopac.com/2017/05/22/sterile-materials-and-outcomes-for-3d-printing-sterile-parts/. Accessed 30 Apr 2020
138. Beckwith AL, Velásquez-García LF, Borenstein JT (2019) Microfluidic model for evaluation of immune checkpoint inhibitors in human tumors. Adv Healthc Mater 8:1900289. https://doi.org/10.1002/adhm.201900289
139. Smith LJ, Li P, Holland MR, Ekser B (2018) FABRICA: a bioreactor platform for printing, perfusing, observing, & stimulating 3D tissues. Sci Rep 8:1–10. https://doi.org/10.1038/s41598-018-25663-7
140. Ochs CJ, Kasuya J, Pavesi A, Kamm RD (2014) Oxygen levels in thermoplastic microfluidic devices during cell culture. Lab Chip 14:459–462. https://doi.org/10.1039/c3lc51160j
141. Kim L, Toh YC, Voldman J, Yu H (2007) A practical guide to microfluidic perfusion culture of adherent mammalian cells. Lab Chip 7:681–694. https://doi.org/10.1039/b704602b
142. Bhise NS, Manoharan V, Massa S, Tamayol A, Ghaderi M, Miscuglio M, Lang Q, Zhang YS, Shin SR, Calzone G, Annabi N, Shupe TD, Bishop CE, Atala A, Dokmeci MR, Khademhosseini A (2016) A liver-on-a-chip platform with bioprinted hepatic spheroids. Biofabrication 8:014101. https://doi.org/10.1088/1758-5090/8/1/014101
143. Kolesky DB, Homan KA, Skylar-Scott MA, Lewis JA (2016) Three-dimensional bioprinting of thick vascularized tissues. Proc Natl Acad Sci 113:3179–3184. https://doi.org/10.1073/PNAS.1521342113
144. Gu Q, Tomaskovic-Crook E, Lozano R, Chen Y, Kapsa RM, Zhou Q, Wallace GG, Crook JM (2016) Functional 3D neural mini-tissues from printed gel-based bioink and human neural stem cells. Adv Healthc Mater 5:1429–1438. https://doi.org/10.1002/adhm.201600095
145. Ma X, Qu X, Zhu W, Li YS, Yuan S, Zhang H, Liu J, Wang P, Lai CSE, Zanella F, Feng GS, Sheikh F, Chien S, Chen S (2016) Deterministically patterned biomimetic human iPSC-derived hepatic model via rapid 3D bioprinting. Proc Natl Acad Sci U S A 113:2206–2211. https://doi.org/10.1073/pnas.1524510113
146. Jang K-J, Otieno MA, Ronxhi J, Lim H-K, Ewart L, Kodella KR, Petropolis DB, Kulkarni G, Rubins JE, Conegliano D, Nawroth J, Simic D, Lam W, Singer M, Barale E, Singh B, Sonee M, Streeter AJ, Manthey C, Jones B, Srivastava A, Andersson LC, Williams D, Park H, Barrile R, Sliz J, Herland A, Haney S, Karalis K, Ingber DE, Hamilton GA (2019) Reproducing human and cross-species drug toxicities using a liver-chip. Sci Transl Med 11:5516. https://doi.org/10.1126/scitranslmed.aax5516
147. Park TE, Mustafaoglu N, Herland A, Hasselkus R, Mannix R, FitzGerald EA, Prantil-Baun R, Watters A, Henry O, Benz M, Sanchez H, McCrea HJ, Goumnerova LC, Song HW, Palecek SP, Shusta E, Ingber DE (2019) Hypoxia-enhanced blood-brain barrier chip recapitulates human barrier function and shuttling of drugs and antibodies. Nat Commun 10:1–12. https://doi.org/10.1038/s41467-019-10588-0
148. Chou DB, Frismantas V, Milton Y, David R, Pop-Damkov P, Ferguson D, MacDonald A, Vargel Bölükbaşı Ö, Joyce CE, Moreira Teixeira LS, Rech A, Jiang A, Calamari E, Jalili-Firoozinezhad S, Furlong BA, O'Sullivan LR, Ng CF, Choe Y, Marquez S, Myers KC, Weinberg OK, Hasserjian RP, Novak R, Levy O, Prantil-Baun R, Novina CD, Shimamura A, Ewart L, Ingber DE (2020) On-chip recapitulation of clinical bone marrow toxicities and patient-specific pathophysiology. Nat Biomed Eng 4:394–406. https://doi.org/10.1038/s41551-019-0495-z
149. Benam KH, Villenave R, Lucchesi C, Varone A, Hubeau C, Lee HH, Alves SE, Salmon M, Ferrante TC, Weaver JC, Bahinski A, Hamilton GA, Ingber DE (2016) Small airway-on-a-chip enables analysis of human lung inflammation and drug responses in vitro. Nat Methods 13:151–157. https://doi.org/10.1038/nmeth.3697
150. Bakarich SE, Gorkin R, Gately R, Naficy S, in het PanhuisSpinks MGM (2017) 3D printing of tough hydrogel composites with spatially varying materials properties. Addit Manuf 14:24–30. https://doi.org/10.1016/j.addma.2016.12.003
151. Mogas-Soldevila L, Duro-Royo J, Oxman N (2016) Water-based robotic fabrication: large-scale additive manufacturing of functionally graded hydrogel composites via multichamber extrusion. 3D Print Addit Manuf 1:141–151. https://doi.org/10.1089/3dp.2014.0014
152. Ober TJ, Foresti D, Lewis JA (2015) Active mixing of complex fluids at the microscale. Proc Natl Acad Sci U S A 112:12293–12298. https://doi.org/10.1073/pnas.1509224112
153. Elbaz A, He Z, Gao B, Chi J, Su E, Zhang D, Liu S, Xu H, Liu H, Gu Z (2018) Recent biomedical applications of bio-sourced materials. Bio-Design Manuf 1:26–44. https://doi.org/10.1007/s42242-018-0002-5
154. Moeinzadeh S, Pajoum Shariati SR, Jabbari E (2016) Comparative effect of physicomechanical and biomolecular cues on zone-specific chondrogenic differentiation of mesenchymal stem cells. Biomaterials 92:57–70. https://doi.org/10.1016/j.biomaterials.2016.03.034
155. Jung JW, Lee JS, Cho DW (2016) Computer-aided multiple-head 3D printing system for printing of heterogeneous organ/tissue constructs. Sci Rep 6:1–9. https://doi.org/10.1038/srep21685

156. Ashammakhi N, Ahadian S, Xu C, Montazerian H, Ko H, Nasiri R, Barros N, Khademhosseini A (2019) Bioinks and bioprinting technologies to make heterogeneous and biomimetic tissue constructs. Mater Today Bio 1:100008. https://doi.org/10.1016/j.mtbio.2019.100008
157. Discher DE, Mooney DJ, Zandstra PW (2009) Growth factors, matrices, and forces combine and control stem cells. Science (80-) 324:1673–1677. https://doi.org/10.1126/science.1171643
158. Kshitiz PJ, Kim P, Helen W, Engler AJ, Levchenko A, Kim DH (2012) Control of stem cell fate and function by engineering physical microenvironments. Integr Biol UK 4:1008–1018. https://doi.org/10.1039/c2ib20080e
159. Xing F, Li L, Zhou C, Long C, Wu L, Lei H, Kong Q, Fan Y, Xiang Z, Zhang X (2019) Regulation and directing stem cell fate by tissue engineering functional microenvironments: scaffold physical and chemical cues. Stem Cells Int. https://doi.org/10.1155/2019/2180925
160. Shi X, Zhou J, Zhao Y, Li L, Wu H (2013) Gradient-regulated hydrogel for interface tissue engineering: steering simultaneous osteo/chondrogenesis of stem cells on a chip. Adv Healthc Mater 2:846–853. https://doi.org/10.1002/adhm.201200333
161. Engler AJ, Sen S, Sweeney HL, Discher DE (2006) Matrix elasticity directs stem cell lineage specification. Cell 126:677–689. https://doi.org/10.1016/j.cell.2006.06.044
162. Chrzanowska-Wodnicka M, Burridge K (1996) Rho-stimulated contractility drives the formation of stress fibers and focal adhesions. J Cell Biol 133:1403–1415. https://doi.org/10.1083/jcb.133.6.1403
163. Lessey EC, Guilluy C, Burridge K (2012) From mechanical force to RhoA activation. Biochemistry 51:7420–7432. https://doi.org/10.1021/bi300758e
164. Watanabe N, Kato T, Fujita A, Ishizaki T, Narumiya S (1999) Cooperation between mDia1 and ROCK in rho-induced actin reorganization. Nat Cell Biol 1:136–143. https://doi.org/10.1038/11056
165. Bhadriraju K, Yang M, Ruiz SA, Pirone D, Tan J, Chen CS (2007) Activation of ROCK by RhoA is regulated by cell adhesion, shape, and cytoskeletal tension. Exp Cell Res. https://doi.org/10.1016/J.YEXCR.2007.07.002
166. McBeath R, Pirone DM, Nelson CM, Bhadriraju K, Chen CS (2004) Cell shape, cytoskeletal tension, and RhoA regulate stem cell lineage commitment. Dev Cell 6:483–495. https://doi.org/10.1016/S1534-5807(04)00075-9
167. Keselowsky BG, Collard DM, García AJ (2005) Integrin binding specificity regulates biomaterial surface chemistry effects on cell differentiation. Proc Natl Acad Sci U S A 102:5953–5957. https://doi.org/10.1073/pnas.0407356102
168. Benoit DSW, Schwartz MP, Durney AR, Anseth KS (2008) Small functional groups for controlled differentiation of hydrogel-encapsulated human mesenchymal stem cells. Nat Mater 7:816–823. https://doi.org/10.1038/nmat2269
169. Jaidev LR, Chatterjee K (2019) Surface functionalization of 3D printed polymer scaffolds to augment stem cell response. Mater Des 161:44–54. https://doi.org/10.1016/j.matdes.2018.11.018
170. Wang P, Zhao L, Liu J, Weir MD, Zhou X, Xu HHK (2015) Bone tissue engineering via nanostructured calcium phosphate biomaterials and stem cells. Bone Res 2:1–13. https://doi.org/10.1038/boneres.2014.17
171. Chen X, Wang J, Chen Y, Cai H, Yang X, Zhu X, Fan Y, Zhang X (2016) Roles of calcium phosphate-mediated integrin expression and MAPK signaling pathways in the osteoblastic differentiation of mesenchymal stem cells. J Mater Chem B 4:2280–2289. https://doi.org/10.1039/c6tb00349d
172. Tang Z, Wang Z, Qing F, Ni Y, Fan Y, Tan Y, Zhang X (2015) Bone morphogenetic protein Smads signaling in mesenchymal stem cells affected by osteoinductive calcium phosphate ceramics. J Biomed Mater Res Part A 103:1001–1010. https://doi.org/10.1002/jbm.a.35242
173. Murphy WL, McDevitt TC, Engler AJ (2014) Materials as stem cell regulators. Nat Mater 13:547–557. https://doi.org/10.1038/nmat3937
174. Guenat OT, Berthiaume F (2018) Incorporating mechanical strain in organs-on-a-chip: lung and skin. Biomicrofluidics 12:042207. https://doi.org/10.1063/1.5024895
175. Occhetta P, Mainardi A, Votta E, Vallmajo-Martin Q, Ehrbar M, Martin I, Barbero A, Rasponi M (2019) Hyperphysiological compression of articular cartilage induces an osteoarthritic phenotype in a cartilage-on-a-chip model. Nat Biomed Eng 3:545–557. https://doi.org/10.1038/s41551-019-0406-3
176. Wallin TJ, Pikul J, Shepherd RF (2018) 3D printing of soft robotic systems. Nat Rev Mater 3:84–100. https://doi.org/10.1038/s41578-018-0002-2
177. Cianchetti M, Laschi C, Menciassi A, Dario P (2018) Biomedical applications of soft robotics. Nat Rev Mater 3:143–153. https://doi.org/10.1038/s41578-018-0022-y
178. Sun L, Chen Z, Bian F, Zhao Y (2020) Bioinspired soft robotic caterpillar with cardiomyocyte drivers. Adv Funct Mater 30:1907820. https://doi.org/10.1002/adfm.201907820
179. Aboulkheyr Es H, Montazeri L, Aref AR, Vosough M, Baharvand H (2018) Personalized cancer medicine: an organoid approach. Trends Biotechnol 36:358–371. https://doi.org/10.1016/j.tibtech.2017.12.005
180. Astolfi M, Péant B, Lateef MA, Rousset N, Kendall-Dupont J, Carmona E, Monet F, Saad F, Provencher D, Mes-Masson AM, Gervais T (2016) Micro-dissected tumor tissues on chip: an ex vivo method for drug testing and personalized therapy. Lab Chip 16:312–325. https://doi.org/10.1039/c5lc01108f
181. Moore N, Doty D, Zielstorff M, Kariv I, Moy LY, Gimbel A, Chevillet JR, Lowry N, Santos J, Mott V, Kratchman L, Lau T, Addona G, Chen H, Borenstein JT (2018) A multiplexed microfluidic system for evaluation of dynamics of immune-tumor interactions. Lab Chip 18:1844–1858. https://doi.org/10.1039/c8lc00256h
182. Yi HG, Jeong YH, Kim Y, Choi YJ, Moon HE, Park SH, Kang KS, Bae M, Jang J, Youn H, Paek SH, Cho DW (2019) A bioprinted human-glioblastoma-on-a-chip for the identification of patient-specific responses to chemoradiotherapy. Nat Biomed Eng 3:509–519. https://doi.org/10.1038/s41551-019-0363-x